12-27-2010

Biphasic Targeting And Cleavage Furrow Ingression Directed By The Tail Of A Myosin II

X. Fang

J. Y. Luo

R. Nishihama

See next page for additional authors

Biphasic targeting and cleavage furrow ingression directed by the tail of a myosin II

Xiaodong Fang,[1] Jianying Luo,[1] Ryuichi Nishihama,[2] Carsten Wloka,[1,3] Christopher Dravis,[1] Mirko Travaglia,[1] Masayuki Iwase,[1] Elizabeth A. Vallen,[4] and Erfei Bi[1]

[1]Department of Cell and Developmental Biology, University of Pennsylvania School of Medicine, Philadelphia, PA 19104
[2]Department of Genetics, Stanford University of School of Medicine, Stanford, CA 94305
[3]Department of Biology, Chemistry and Pharmacy, Free University of Berlin, D-14195 Berlin, Germany
[4]Department of Biology, Swarthmore College, Swarthmore, PA 19081

Cytokinesis in animal and fungal cells utilizes a contractile actomyosin ring (AMR). However, how myosin II is targeted to the division site and promotes AMR assembly, and how the AMR coordinates with membrane trafficking during cytokinesis, remains poorly understood. Here we show that Myo1 is a two-headed myosin II in *Saccharomyces cerevisiae*, and that Myo1 localizes to the division site via two distinct targeting signals in its tail that act sequentially during the cell cycle. Before cytokinesis, Myo1 localization depends on the septin-binding protein Bni5. During cytokinesis, Myo1 localization depends on the IQGAP Iqg1. We also show that the Myo1 tail is sufficient for promoting the assembly of a "headless" AMR, which guides membrane deposition and extracellular matrix remodeling at the division site. Our study establishes a biphasic targeting mechanism for myosin II and highlights an underappreciated role of the AMR in cytokinesis beyond force generation.

Introduction

Cytokinesis in animal and fungal cells is performed by the concerted action of a contractile actomyosin ring (AMR) and targeted membrane deposition coupled with ECM remodeling at the division site (Balasubramanian et al., 2004; Strickland and Burgess, 2004). The AMR, which consists of myosin II and actin filaments, is thought to be the engine that drives the ingression of the plasma membrane at the division site during cytokinesis. However, important questions regarding the assembly and function of the AMR remain unanswered. For example, how is myosin II targeted to the division site? How does myosin direct actin ring assembly? How does the AMR coordinate with membrane trafficking during cytokinesis?

The budding yeast *Saccharomyces cerevisiae* provides an excellent system for structure–function analysis of myosin II and for determining its role in cytokinesis, as deletion of *MYO1*, the sole myosin II in budding yeast, does not cause cell lethality in most strain backgrounds but produces serious defects in cytokinesis and cell separation (Bi et al., 1998; Schmidt et al., 2002), permitting the in vivo analysis of a variety of *myo1* mutations. However, the structure of Myo1 is not known. In this study, we show by rotary-shadowing electron microscopy (EM) that Myo1 forms a dimer with a kink in its tail, similar to myosin IIs in other eukaryotic cells.

To understand the function of a myosin II in cytokinesis, it is important to understand how it is targeted to the division site. Studies in multiple systems indicate that the targeting signals for cleavage-furrow localization reside in the tails of myosin IIs (Sabry et al., 1997; Motegi et al., 2004; Lord et al., 2005; Lister et al., 2006; Beach and Egelhoff, 2009; Ronen and Ravid, 2009). In addition, some proteins, such as Mid1, an anillin-related protein in fission yeast (Motegi et al., 2004; Wu et al., 2006; Huang et al., 2008), and the septins, a family of GTP-binding, filament-forming proteins (Longtine and Bi, 2003; Joo et al., 2005) in budding yeast (Bi et al., 1998; Lippincott and Li, 1998) and mammalian cells (Joo et al., 2007), have been implicated in myosin localization during cytokinesis. However, clear mechanisms that account for the entire myosin localization at the division site have not been elucidated in any organism.

In budding yeast, septins play important roles in Myo1 localization (Bi et al., 1998; Lippincott and Li, 1998). However, how

Correspondence to Erfei Bi: ebi@mail.med.upenn.edu

Abbreviations used in this paper: AMR, actomyosin ring; DIC, differential interference contrast; ELC, essential light chain; FOA, fluoroorotic acid; LatA, latrunculin A; MBP, maltose-binding protein; PS, primary septum.

The Rockefeller University Press $30.00
J. Cell Biol. Vol. 191 No. 7 1333–1350
www.jcb.org/cgi/doi/10.1083/jcb.201005134

the septin hourglass recruits and maintains Myo1 at the division site before cytokinesis and how Myo1 is anchored to the neck cortex flanked by two septin rings, which result from septin-hourglass splitting at the onset of mitotic exit (Lippincott et al., 2001), during cytokinesis remain unanswered. In this study, we show that Myo1 is recruited to the division site via a biphasic mechanism involving distinct targeting signals in its tail and distinct molecular pathways.

AMR contraction and membrane trafficking are hallmarks of animal and fungal cytokinesis (Balasubramanian et al., 2004; Strickland and Burgess, 2004). The AMR is thought to generate force that powers plasma membrane ingression, whereas targeted membrane deposition is thought to increase cell surface area and also to deliver cargo enzymes for ECM remodeling at the division site, which results in the formation of chitinous primary septum (PS) in budding yeast. These processes must coordinate in time and space to achieve robust cytokinesis. However, the functional and mechanistic relationships between these processes remain poorly understood. In this study, we present evidence to suggest that the AMR functions as a structural unit to "guide" membrane trafficking and ECM remodeling at the division site. This guidance role can be largely fulfilled without the motor domain of Myo1 in budding yeast, which can explain the striking observation made previously that the Myo1 tail is sufficient to support cytokinesis (Lord et al., 2005). The generality of the guidance concept and the motor-independent role of the AMR in cytokinesis are discussed.

Results

Myo1 is a two-headed myosin with a kink in its tail

To determine the structure of full-length Myo1, we purified a C-terminally TAP-tagged Myo1 from yeast cells, expressed under its own promoter (Fig. 1 A). The TAP-tagged Myo1 construct appears to function normally, as it did not cause any defects in cytokinesis and cell separation (unpublished data). We determined its structure by rotary-shadowing EM. Myo1 formed dimers, each with two globular heads and a rod tail (Fig. 1 A). The average length of Myo1 tail (1073 aa, residues 856–1928) was 126 ± 12 nm (n = 41). In addition, 56% of Myo1 dimers displayed a clear "kink" or "hinge" in their tails, located at 46 ± 6 nm from the head–tail junction, which corresponds to the predicted helix-breaking region (236 aa, residues 1176–1411) in Myo1 tail (Fig. S1). To further validate the Myo1 structure and confirm the kink position in its tail, a C-terminally TAP-tagged Myo1 with a deletion of the TD2 region (174 aa, residues 1224–1397; see next section) that contains all seven helix-breaking prolines in Myo1 tail (Fig. S1, red bar) was purified and its structure was determined. The tail length (118 ± 12 nm, n = 39) of Myo1-TD2Δ was reduced proportionally (Fig. 1 A), and the number of Myo1-TD2Δ dimers with kinked tails was also reduced to 31%, with the kink located at 41 ± 10 nm from the head–tail junction. The TD2 accounts for only a portion of the predicted helix-breaking region, which may explain why deletion of the TD2 reduced, but did not eliminate, the propensity of the Myo1 tail to form a kink.

To determine whether the Myo1 tail is sufficient for dimerization in vitro, Myo1 tail lacking the TD2 region was fused to maltose-binding protein (MBP), a known globular protein. MBP-Myo1-tail-TD2Δ was purified from *Escherichia coli* (Fig. 1 B) and its structure was visualized by rotary-shadowing EM. Again, MBP-Myo1-tail-TD2Δ molecules formed a "two-headed" structure with a kinked tail (Fig. 1 B).

Together, these data demonstrate that Myo1 is a two-headed myosin II, resembling "conventional" myosins in other eukaryotes. In addition, Myo1 has a clear kink in its tail, similar to myosin IIs from *Dictyostelium*, *Acanthamoeba*, smooth muscle, and nonmuscle cells (Trybus, 1991).

Myo1 tail contains two temporally distinct targeting domains

To identify potential targeting domains in Myo1, we constructed functional N- and C-terminally *GFP*-tagged *MYO1* alleles and used them to make internal or terminal deletions of *MYO1*, leading to the identification of two distinct targeting domains, mTD1 (minimal targeting domain 1) and TD2 (targeting domain 2), in Myo1 tail (Fig. 1 C). Myo1 head or any other region of Myo1 tail did not localize to the division site in *myo1*Δ cells, suggesting that mTD1 and TD2 are the only targeting domains of Myo1. A third region, the putative "assembly domain" (AD) allowed localization only in the presence of endogenous Myo1 (Fig. 1 C). Strikingly, mTD1 localized to the division site in small- to large-budded cells, whereas TD2 localized to the division site only in large-budded cells (Fig. 1 D). Live-cell imaging further demonstrates that mTD1 and TD2 mediate Myo1 localization before and during cytokinesis, respectively (see Fig. 4 A). Thus, Myo1 tail contains two temporally distinct targeting domains.

Myo1 targeting before cytokinesis depends on the septin-binding protein Bni5

Myo1 localization to the bud neck depends on the septins (Bi et al., 1998; Lippincott and Li, 1998). In addition, Myo1 tail carried on a high-copy plasmid suppressed the growth defect of various temperature-sensitive septin mutants (unpublished data), suggesting a close functional association of Myo1 with the septins. However, in vitro protein-binding assays using recombinant Myo1 targeting domains (MBP, MBP-TD1, MBP-mTD1, and MBP-TD2) and septin complexes (Cdc3, Cdc10, Cdc11, and HisX6-Cdc12) failed to detect a convincing interaction between Myo1-TDs and the septins, which raises the possibility that a "linker protein" may be involved in Myo1–septin interaction.

Bni5 localizes to the bud neck in a septin-dependent manner from bud emergence in late G1 to spindle disassembly in telophase, which coincides with the onset of cytokinesis (Lee et al., 2002). In addition, both Bni5 and Myo1 appear to function in the same genetic pathway (Lee et al., 2002). These observations raise the possibility that Bni5 may link Myo1 to the septins before cytokinesis. To test this possibility, GFP-tagged Myo1, mTD1, and TD2 were visualized in wild-type and *bni5*Δ cells. Strikingly, the full-length Myo1 localized to the division site only in large-budded *bni5*Δ cells, whereas the localization

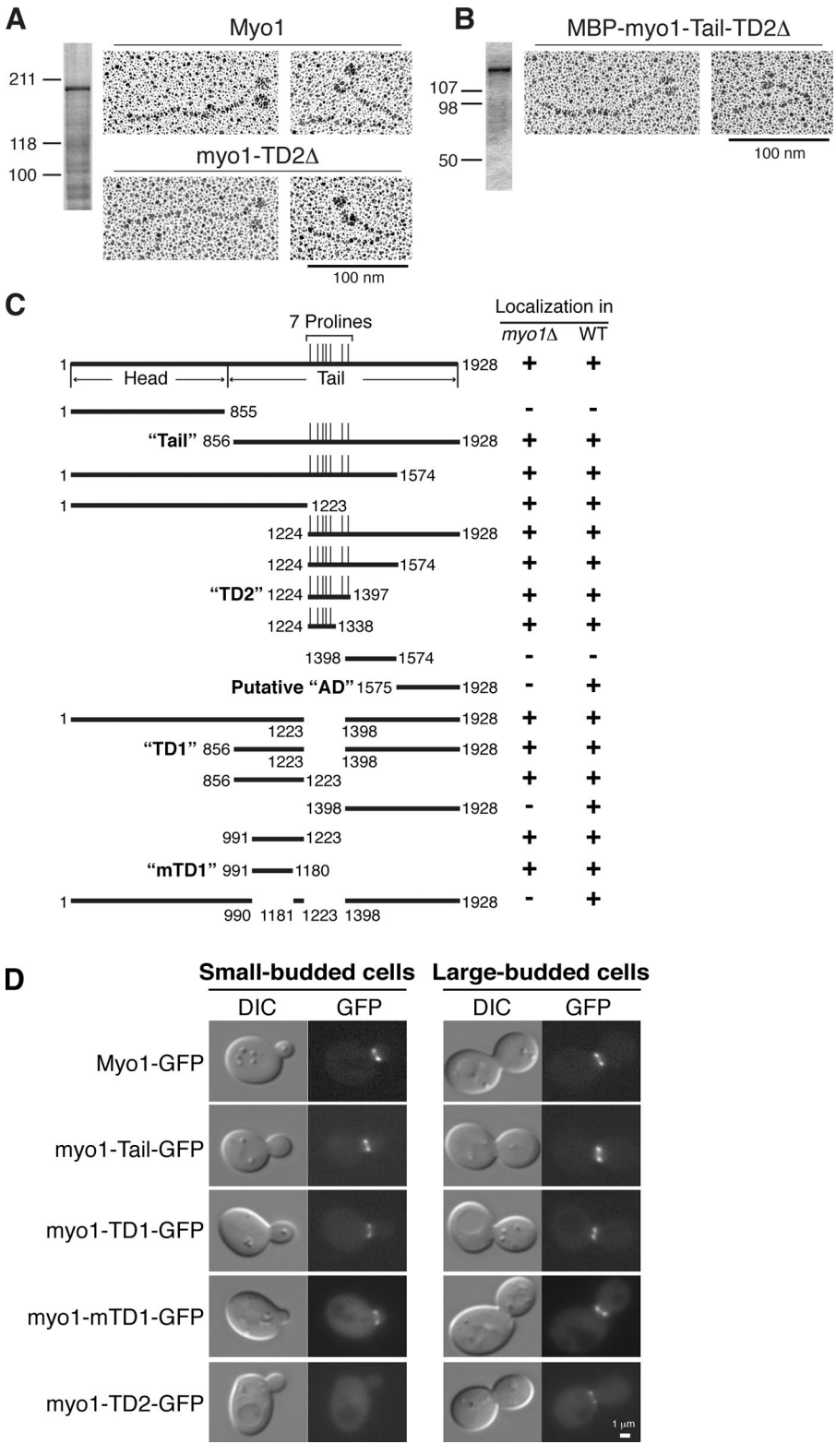

Figure 1. **Myo1 is a two-headed myosin and its tail contains two distinct targeting domains.** (A) Myo1 heavy chain forms a dimer in yeast. Myo1-C-TAP and myo1-TD2Δ-C-TAP were purified from strains XDY7 and XDY99, respectively (left, silver staining), and observed by rotary-shadowing EM (right). (B) Recombinant myo1-Tail forms a dimer. MBP-myo1-Tail-TD2Δ was purified from *E. coli* (left, Coomassie blue staining) and observed by rotary-shadowing EM (right). (C) Summary of localization data on Myo1 fragments. mTD1, minimal targeting domain 1; TD2, targeting domain 2; AD, assembly domain. (D) Localization of different Myo1 fragments during the cell cycle. Yeast strains (XDY41, YJL335A, YJL221A, YJL489A, YJL222A; see Table II) were used for observation. Bar, 1 μm.

of mTD1 at the division site was completely eliminated (Fig. 2 A). In contrast, the localization of TD2 at the division site was unaffected by *bni5*Δ (Fig. S2 A). Consistently, Bni5 colocalized with the full-length Myo1 at the bud neck until the onset of Myo1 ring constriction (Fig. 2 B, left; Video 1, left), whereas Bni5 and the mTD1 colocalized at and co-disappeared from the bud neck precisely before cytokinesis (Fig. 2 B, right; Video 1, right). These results demonstrate that Myo1 targeting before cytokinesis completely depends on Bni5.

To determine whether Myo1 and Bni5 interact directly, co-immunoprecipitation and in vitro protein-binding assays were performed. Myo1 tail fragments containing the mTD1 region (Tail, TD1, and mTD1; see Fig. 1 C), but not TD2 or the putative AD, interacted with Bni5 in yeast cell lysates (Fig. 2 C). Recombinant

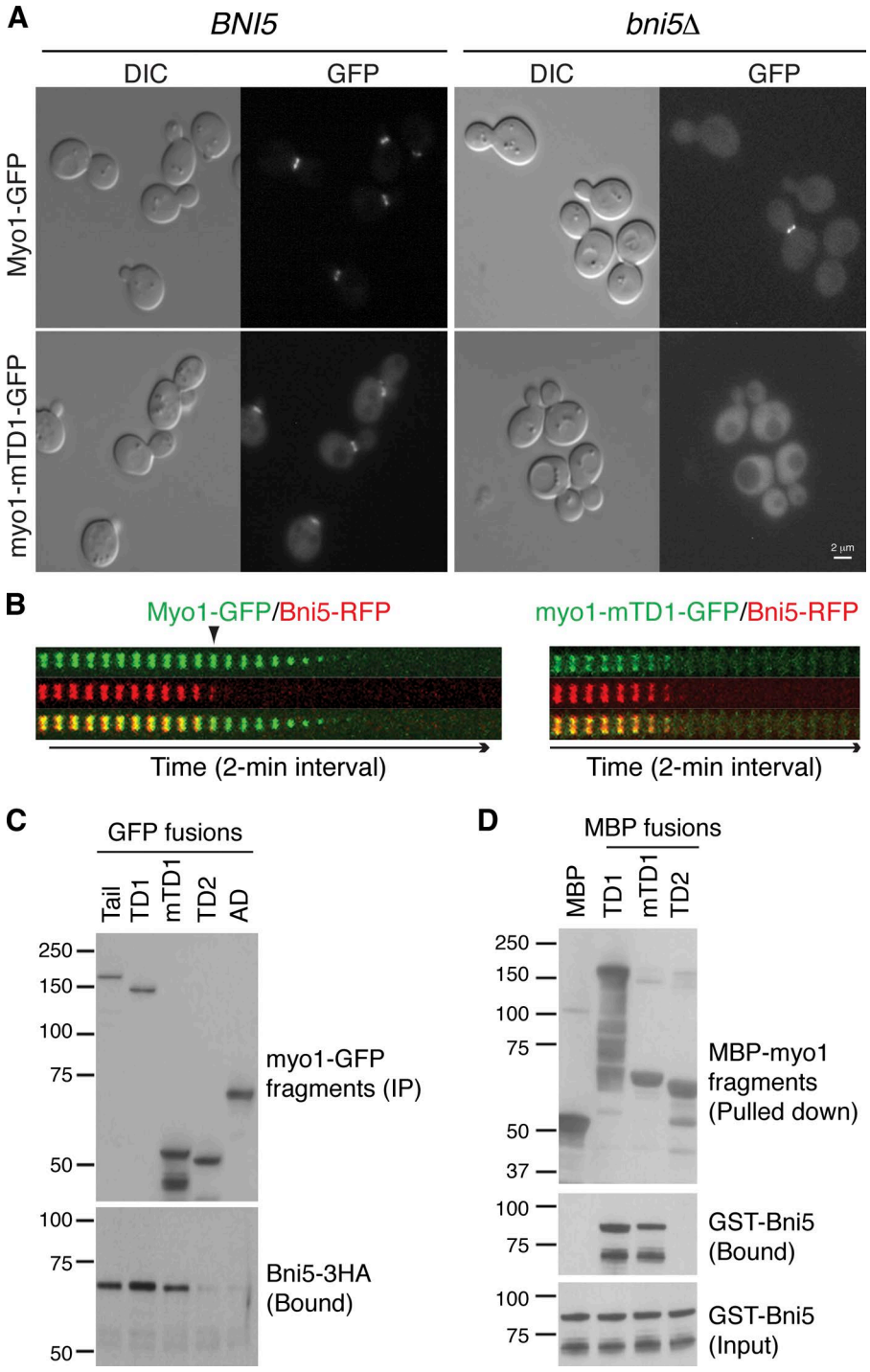

Figure 2. **Myo1 targeting before cytokinesis depends on its interaction through mTD1 with Bni5.** (A) Localization of Myo1 and myo1-mTD1 in wild-type and *bni5*Δ cells. Cells carrying *MYO1-GFP* or *myo1-mTD1-GFP* in wild-type (*BNI5*) (YXD41 and YJL489A) or *bni5*Δ (XDY254 and XDY258) backgrounds were grown in YPD at 23°C and observed by DIC and fluorescence microscopy. (B) Strains YEF6321 (*MYO1-GFP BNI5-RFP*; left) and YEF6326 (*myo1-mTD1-GFP BNI5-RFP*; right) were grown in YPD at 23°C and then imaged by 3D dual-color time-lapse microscopy at 23°C with a 2-min interval. Montage images of the GFP, RFP, and merged channels from the representative time-lapse data are shown here. Arrowhead indicates the start of Myo1 ring constriction. (C) myo1-mTD1 interacts with Bni5 in yeast. GFP-tagged Myo1 fragments were immunoprecipitated using anti-GFP antibody from cell lysates of yeast strains (XDY189, XDY190, XDY191, XDY192, and XDY194; see Table II). Myo1 fragments (IP) and Bni5-3HA (Bound) in the precipitates were detected by Western blot analyses using antibodies against GFP and HA, respectively. (D) myo1-mTD1 interacts with Bni5 in vitro. Equal amounts of MBP, MBP-myo1-TD1, MBP-myo1-mTD1, and MBP-myo1-TD2 bound to amylose beads were mixed individually with the same amount of GST-Bni5. The pulled down MBP and MBP-myo1 fragments as well as GST-Bni5 in the bound and input fractions were detected by Western blot analyses using antibodies against MBP and GST, respectively.

MBP-TD1 and MBP-mTD1 interacted directly with recombinant GST-Bni5 (Fig. 2 D). In contrast, MBP or MBP-TD2 failed to interact with GST-Bni5. As previous results have demonstrated that Bni5 binds to the septin Cdc11 (Lee et al., 2002), these data establish Bni5 as a direct molecular linker between the septins and Myo1 (Septins → Bni5 → Myo1 [mTD1]) before cytokinesis.

Myo1 targeting during cytokinesis depends on ELC and IQGAP

The timing of TD2 localization is similar to that of actin ring assembly (Epp and Chant, 1997; Bi et al., 1998; Lippincott and Li, 1998). However, the TD2 still localized to the division site when cells were treated with latrunculin A (Fig. S2 B), a drug that disrupts all F-actin structures including the actin ring (Ayscough et al., 1997), suggesting that the TD2-mediated Myo1 targeting may involve proteins other than F-actin. A number of cytokinesis proteins such as Mlc1, Iqg1, Hof1, Cyk3, Inn1, and Chs2 localize to the division site before or around the time of TD2 localization, making them candidates for TD2-mediated Myo1 targeting. Strikingly, the TD2-GFP, carried on a plasmid, completely failed to localize in *mlc1-11* and *iqg1*Δ cells but still localized in other cytokinesis mutants

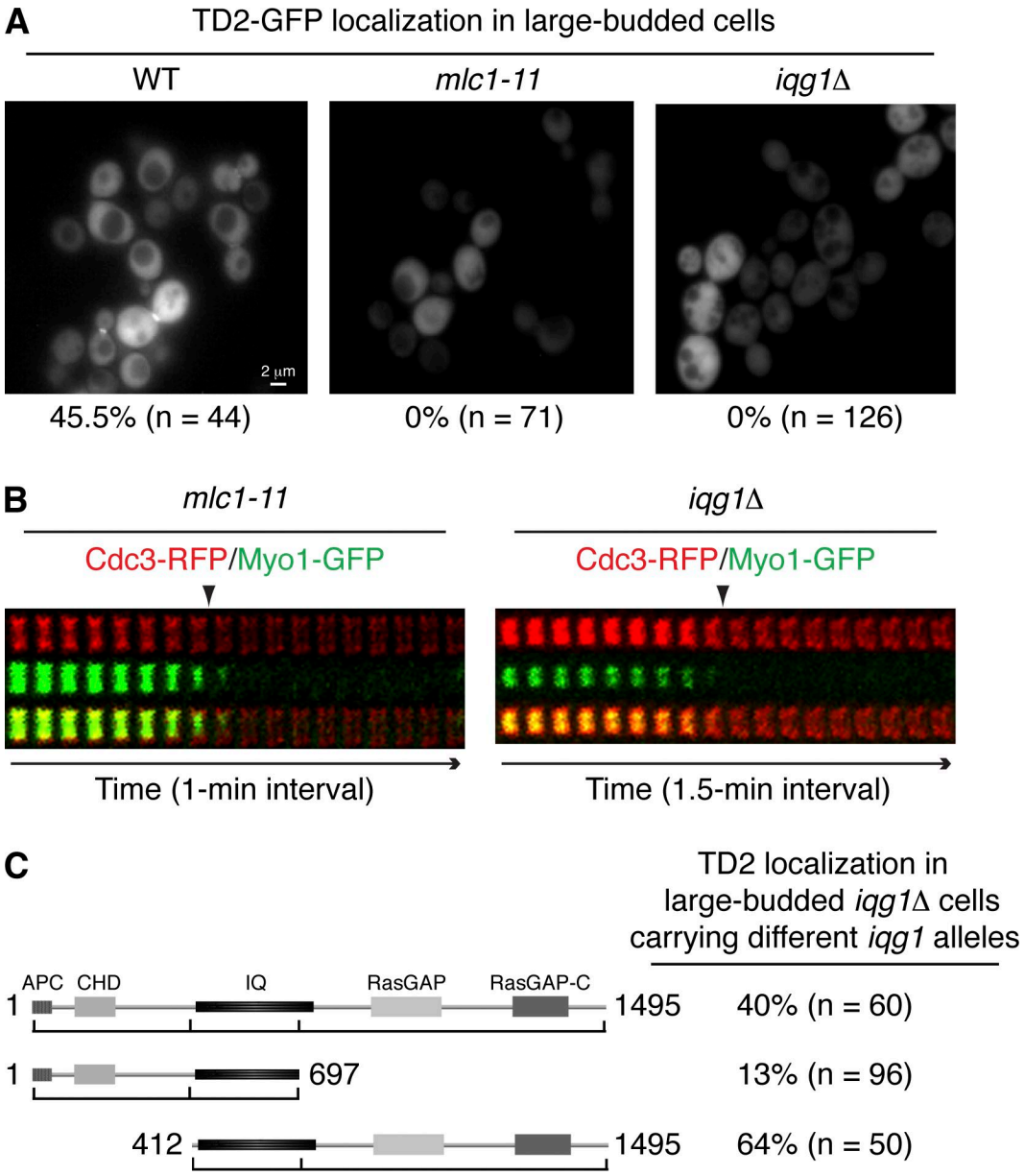

Figure 3. **Myo1 targeting during cytokinesis depends on Mlc1 and Iqg1.** (A) myo1-TD2 localization depends on Mlc1 and Iqg1. Wild-type (WT) (XDY154), *mlc1-11* (XDY173), and *iqg1*Δ (XDY218) cells carrying plasmid pRS316-MYO1-TD2-GFP were grown in SC-Ura medium at 23°C and then examined for myo1-TD2 localization. (B) Full-length Myo1 localization depends on Mlc1 and Iqg1. Strains YEF6179 (*mlc1-11 MYO1-GFP CDC3-RFP*; left) and YEF6325 (*iqg1*Δ *CDC3-RFP*, pRS316-MYO1-C-GFP; right) were grown in liquid SC-Leu media at 23°C and then imaged by 3D dual-color time-lapse microscopy at 23°C with indicated intervals. Montage images of the GFP, RFP, and merged channels from the representative time-lapse data are shown here. Arrowheads indicate the splitting of septin hourglass into two cortical rings, which coincides with mitotic exit and the onset of cytokinesis. (C) myo1-TD2 localization in cells containing different *iqg1* alleles. Plasmid pRS315 derivatives carrying the indicated *iqg1* alleles (see Table III) were transformed into strain XDY218. Transformants were grown in SC-Ura-Leu medium at 23°C and then quantified for myo1-TD2 localization. APC, APC/C recognition site; CHD, calponin-homology domain; IQ, IQ motifs; Ras-GAP, RasGAP-related domain; RasGAP-C, RasGAP C terminus–related domain.

(*hof1*Δ, *cyk3*Δ, *hof1*Δ *cyk3*Δ, *inn1*Δ, and *chs2*Δ; all these strains contain the endogenous *MYO1*; Fig. 3 A and unpublished data). More importantly, the GFP-tagged full-length Myo1 disappeared from the bud neck in *mlc1-11* and *iqg1*Δ cells precisely at the time of septin-hourglass splitting (Fig. 3 B; Video 2), which coincides with the onset of mitotic exit or cytokinesis (Lippincott et al., 2001). Thus, the TD2-mediated Myo1 targeting depends on Mlc1 (the ELC [essential light chain] for Myo1) and Iqg1 (IQGAP; Shannon and Li, 2000; Luo et al., 2004). The N-terminal region of Iqg1, which contains an APC recognition site (Ko et al., 2007; Tully et al., 2009) and a CHD (calponin-homology domain; Shannon and Li, 1999), was dispensable for TD2 localization (Fig. 3 C). To date, we failed to detect a convincing interaction between different Iqg1 fragments and the TD2 by two-hybrid and in vitro protein-binding assays (unpublished data), which may reflect complex regulation of this interaction or an interaction that is bridged by other proteins in vivo. Nonetheless, our results, together with the previous observation that Mlc1 binds to the IQ motifs of Iqg1 and is required for the localization of

Iqg1 to the division site (Shannon and Li, 2000), establish a pathway (ELC → IQGAP → Myo1 [TD2]) for Myo1 targeting during cytokinesis.

Distinct targeting mechanisms account for distinct Myo1 localization patterns and dynamics during the cell cycle

To determine how different targeting mechanisms affect Myo1 localization patterns and dynamics during the cell cycle, we performed 3D time-lapse analyses on cells with intact targeting mechanisms or with one mechanism selectively inactivated. In these experiments, all mutant alleles of *MYO1* were the sole source of Myo1 in the cell. Although the overall localization pattern of Myo1 tail, which contains both targeting signals, was similar to that of full-length Myo1 (Fig. 4 A), several differences were noted. Myo1 tail displayed a 21% decrease in the rate of ring "constriction" (Fig. 4 B; Lord et al., 2005; constriction refers to a reduction in the size of Myo1 ring and does not imply the involvement of an actomyosin-based contractile force), and also a defect in ring disassembly (Fig. 4 A; Fig. S3 A; Video 3, compare right to left). Some *myo1-Tail* cells displayed asymmetric or partial ring constriction (Fig. S3 B). These data indicate that Myo1 head accounts for about one fifth of the constriction rate of the Myo1 ring during cytokinesis and also suggest that Myo1 head contributes to Myo1 disassembly during and toward the end of cytokinesis.

To determine the precise timing and dynamics of Myo1 localization conferred by the early targeting mechanism, we examined *myo1-TD2*Δ*-GFP* cells where the region sufficient for late targeting of Myo1 is deleted. myo1-TD2Δ-GFP localized to the incipient bud site and the bud neck as full-length Myo1-GFP did, but its intensity began to fade ∼10–15 min before and disappeared completely from the division site without any constriction around the time of septin-hourglass splitting (Fig. 4, A and B; Video 4), which marks the onset of mitotic exit (telophase–G1 transition; Lippincott et al., 2001). As expected, myo1-TD2Δ-GFP failed to localize to the bud neck in *bni5*Δ cells throughout the cell cycle (Video 5). These data indicate that the early targeting mechanism of Myo1 is responsible for its localization from late G1 to telophase, and this targeting event completely depends on Bni5.

To determine the precise timing and dynamics of Myo1 localization conferred by the late targeting mechanism, we examined two complementary situations. In *bni5*Δ cells where the early targeting mechanism is eliminated (Fig. 2, A and B), full-length Myo1 began to appear at the division site ∼15 min and reached maximal intensity ∼5 min before septin-hourglass splitting, and then Myo1 ring constricted with a decreased rate but did not linger around the division site after cytokinesis (Fig. 4, A and B; Video 6, left). These data further demonstrate the role of Bni5 in the early targeting of Myo1, and suggest that the late targeting mechanism of Myo1 is responsible for its localization from anaphase to the completion of cytokinesis.

In a complementary experiment, myo1-TD2-GFP alone localized to the division site in a pattern that parallels that of Myo1 in *bni5*Δ cells during the cell cycle (Fig. 4 A). However, in contrast to Myo1 tail or full-length Myo1 in *bni5*Δ cells, very few cells containing myo1-TD2-GFP displayed complete and symmetric ring constriction (Fig. S3 B; Video 6, middle and right). These data indicate that the TD2 is sufficient for Myo1 targeting but not its function during cytokinesis.

In summary, we have established a biphasic targeting mechanism for Myo1 during the cell cycle. The early targeting mechanism accounts for Myo1 localization from late G1 to telophase, which reflects the localization pattern of Bni5 during the cell cycle (Lee et al., 2002; Fig. 2 B). In contrast, the late targeting mechanism accounts for Myo1 localization from anaphase to the completion of cytokinesis, which reflects the localization pattern of Iqg1 during the cell cycle (Epp and Chant, 1997; Lippincott and Li, 1998). These two targeting events overlap from anaphase to telophase when Bni5 and Iqg1 coexist at the bud neck.

Myo1 tail is sufficient for directing actomyosin ring assembly and primary septum formation during cytokinesis

To determine the functional consequences of the distinct targeting mechanisms for Myo1, we examined the effects of inactivating each of the mechanisms on the execution of cytokinesis by examining cell cluster formation, which is indicative of a failure in cytokinesis and/or cell separation. As observed previously (Lord et al., 2005), *myo1-Tail* cells, possessing both targeting domains, displayed a mild defect in cytokinesis (Fig. 5 A). Similarly, *bni5*Δ cells, in which the early targeting of Myo1 is eliminated, displayed little defect in cytokinesis, suggesting that the late targeting of Myo1 is largely responsible for its role in cytokinesis. This conclusion is further supported by the observation that *myo1-TD2* cells, containing only the 174-aa late targeting domain, were able to carry out cytokinesis much more efficiently than *myo1*Δ cells did. Surprisingly, *myo1-TD2*Δ cells, in which the mutant myo1 protein disappears invariably by the onset of mitotic exit (Fig. 4 A), were also able to carry out cytokinesis more efficiently than *myo1*Δ cells did, although much poorly than *myo1-tail* cells. This result suggests that Myo1 localization before the onset of mitotic exit also contributes to cytokinesis, which is further corroborated by the striking observation that the *bni5*Δ *myo1-TD2*Δ cells, in which both targeting mechanisms are inactivated, displayed a cytokinesis defect similar to that of *myo1*Δ cells (Fig. 5 A). These data indicate that Myo1 tail is largely sufficient for cytokinesis, and both targeting mechanisms contribute.

To explore the underlying mechanism for the role of Myo1 tail and its targeting domains in cytokinesis, we examined actin ring assembly in various *myo1* mutants. As expected, 98% of wild-type cells with segregated nuclei formed an actin ring, whereas *myo1*Δ cells at the similar stage of the cell cycle did not (Bi et al., 1998). Remarkably, 92% of the *myo1-Tail* cells assembled an actin ring (Fig. 5 B; Fig. S4 A; Video 7), suggesting that Myo1 tail is sufficient for promoting actin ring assembly and/or maintaining actin filaments independently of the head domain, which contains the only known actin-binding site among all myosin IIs. Both targeting domains contribute to actin ring assembly, as cells lacking either were compromised severely in both the frequency and the quality of actin ring

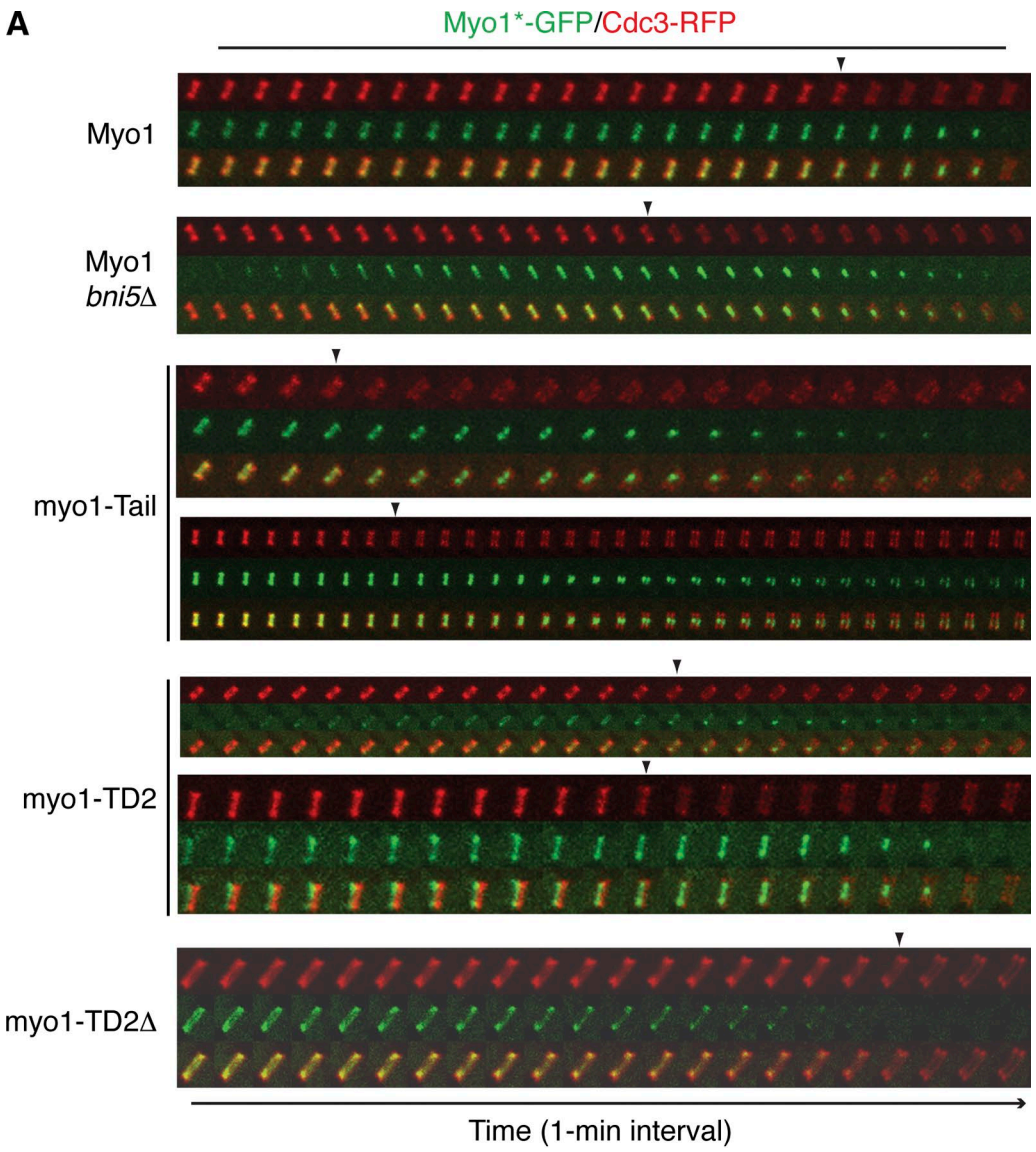

B

	Constriction rate (μm/min)[a]
Myo1:	0.119 +/- 0.020 (n = 27)
Myo1 *bni5*Δ:	0.092 +/- 0.037 (n = 22)
myo1-Tail:	0.094 +/- 0.025 (n = 46)
myo1-TD2Δ:	0.000 +/- 0.00 (n = 42)

Figure 4. **Distinct targeting mechanisms impart distinct Myo1 localization dynamics during the cell cycle.** (A) Effects of *bni5*Δ and *myo1* truncations on the dynamics of Myo1 localization during the cell cycle. Cells of strains XDY286 (*MYO1-GFP*; *n* = 33), XDY287 (*MYO1-GFP bni5*Δ; *n* = 38), XDY288 (*myo1-Tail-GFP*; *n* = 88), XDY289 (*myo1-TD2*Δ*-GFP*; *n* = 42), and XDY290 (*myo1-TD2-GFP*; *n* = 31) were grown in YPD at 23°C and then imaged by 3D dual-color time-lapse microscopy at 23°C with a 1-min interval. Montage images from the representative time-lapse data are shown here. Top row in each image panel: Cdc3-RFP (red); middle row: Myo1*-GFP (asterisk indicates Myo1 or its fragment; green); bottom row: merged images of septin-RFP and Myo1*-GFP. The merged images were used to determine the symmetry of Myo1*-GFP ring during its localization and/or constriction. Arrowheads indicate septin-hourglass splitting. Images within each image panel were processed with the same magnification. (B) Constriction rates of Myo1 and its fragments in wild-type and/or *bni5*Δ cells. "a" indicates that only cells showing symmetric Myo1 constriction were used for the calculation.

assembly. Only 33% and 42% of the *myo1-TD2* and *myo1-TD2*Δ cells formed abnormal actin structures at the division site, which ranged from a smooth actin ring to an amorphous "F-actin cloud" (Fig. S4, A and B). In contrast, 72% of the *bni5*Δ cells formed an actin ring (Fig. S4 A), suggesting a minor

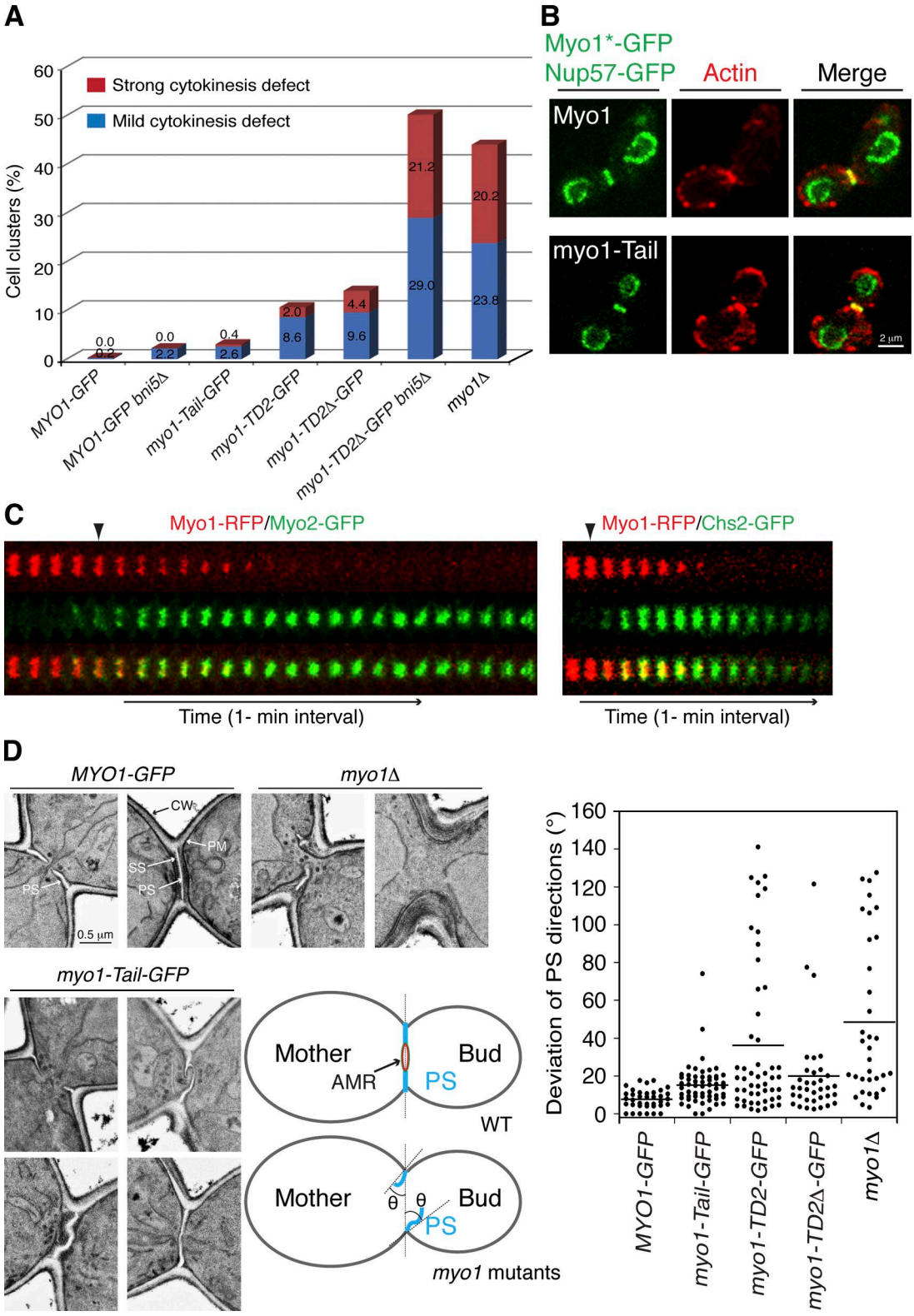

Figure 5. **Motor-independent roles of Myo1 in promoting actin ring assembly and furrow ingression.** (A) Cytokinesis defects in *bni5*Δ and different *myo1* mutants. Cells of strains listed below were grown in YPD at 23°C and scored for cytokinesis defects as follows: mild cytokinesis defect, cells with 3–4 cell bodies linked together; strong cytokinesis defect, cells with more than 4 cell bodies linked together. The number of cells scored for each strain was 500. The strains were XDY41 (*MYO1-GFP*), XDY254 (*MYO1-GFP bni5*Δ), YJL335A (*myo1-Tail-GFP*), YJL222A (*myo1-TD2-GFP*), YJL488A (*myo1-TD2*Δ*-GFP*), YEF6322 (*myo1-TD2*Δ*-GFP bni5*Δ), and YEF1804 (*myo1*Δ). (B) Myo1 tail is sufficient for promoting actin ring assembly. Cells of the strains YEF6307 (*MYO1-GFP NUP57-GFP*; top) and YEF6309 (*myo1-Tail-GFP NUP57-GFP*; bottom) were grown in SC-Ura media at 23°C, fixed, and stained for actin, and then imaged by spinning-disk confocal microscopy along the Z-axis with a 0.1-μm increment (71 and 46 Z-sections for wild-type and *myo1-Tail* cells, respectively). For clear visualization of the actin ring, images of a single focal plane near the middle of the cell were presented (see Video 7 for 3D construction of the actin ring in a *myo1-Tail* cell). Myo1*-GFP indicates GFP-tagged Myo1 or its tail. (C) AMR constriction (marked by Myo1-RFP) is spatiotemporally

Table I. **PS formation in different *myo1* mutants**[a]

PS morphological trait	*MYO1-GFP* (XDY41)	*myo1-Tail-GFP* (YJL335A)	*myo1-TD2-GFP* (YJL222A)	*myo1-TD2Δ-GFP* (YJL488A)	*myo1Δ* (YEF1804)
No PS (= only SS)	0	0	6	12	23
1 PS[b]	57	37	21	30	20
2 PSs	11	25	28	20	14
3 PSs	0	5	10	6	6
4 PSs	0	0	2	0	5
5 PSs	0	1	1	0	0
Total	68	68	68	68	68
PS index[c] (%)	100	100	91	82	66
Neck-spanning index[d] (%)	84	76	23	21	7
PS angles[e] (mean ± SD)	8 ± 5	15 ± 11	36 ± 41	20 ± 24	49 ± 42

[a]Only cells with any sign of septum formation, regardless of its types (PS, primary septum; SS, secondary septum), and with no visible division scars were scored. The latter is to minimize possible mis-scoring of structures from previously formed septa.

[b]An electron-translucent stripe originated from the bud–neck region was defined as one PS.

[c]Number of cells with any PS divided by number of cells with any septum (PS or SS).

[d]Number of cells with a PS spanning the entire bud neck divided by number of cells with any PS.

[e]The angle between two lines starting from the base of a given PS was measured: one line is perpendicular to the mother–bud axis and the other connects to a site along the PS that yields the biggest angle (it could be at the tip or in the middle of the PS). Only cells with one or two PSs that extended at least one quarter of the bud–neck width were used for measurement (see also Fig. 5 D).

contribution of Bni5 to this process. These data indicate that Myo1 tail is sufficient for actin ring assembly, and again, both targeting domains contribute.

How does the "headless" AMR assembled by Myo1 tail drive cytokinesis? In wild-type cells, AMR constriction (marked by Myo1-RFP) and membrane trafficking (marked by myosin V Myo2-GFP) or trafficking-dependent PS formation (marked by chitin synthase Chs2-GFP) are spatiotemporally coupled during cytokinesis (Fig. 5 C; Video 8). Both Myo2 and Chs2 arrive at the division site around septin-hourglass splitting (Fig. S4 C; Video 9), which coincides with the onset of AMR contraction. The AMR has been suggested to guide PS formation and/or cell surface growth in budding yeast (Vallen et al., 2000; Bi, 2001). We tested the possibility that the headless AMR may retain the "guiding role" even in the absence of its motor domain by examining PS formation in various *myo1* mutants using transmission EM (Fig. 5 D; Table I). As expected, wild-type cells formed the PS with high efficiency (100% of the large-budded cells with any septal materials at the division site had a PS) and a sharp orientation (perpendicular to the mother–daughter axis), whereas *myo1*Δ cells formed asymmetric and/or grossly mis-oriented PS with low efficiency (66%). Remarkably, *myo1-tail* cells formed PS with high efficiency (100%) and an orientation close to wild-type cells. Thus, the headless AMR is able to guide PS formation. When either targeting domain was deleted such as in *myo1-TD2* and *myo1-TD2*Δ cells, the efficiency and the orientation of PS formation were severely compromised (Fig. 5 D; Table I). Together, these data demonstrate that Myo1 tail is sufficient for directing AMR assembly and PS formation during cytokinesis.

Both Myo1 and actin filaments are involved in guiding primary septum formation during cytokinesis

The functionality of Myo1 tail in cytokinesis appears to be correlated with its ability to direct actin ring assembly. This raises an interesting possibility that Myo1 tail may simply help actin filaments organize into a ring structure at the division site, and it is the actin filaments that actually direct trafficking and PS formation by capturing and distributing post-Golgi vesicles around the circumference of the division site. The vesicles are delivered to the division site from the Golgi by the myosin V Myo2 along actin cables (Pruyne et al., 1998; Moseley and Goode, 2006). Thus, the actin filaments in actin cables and actin ring, both of which are nucleated by formins (Vallen et al., 2000; Evangelista et al., 2002; Sagot et al., 2002; Tolliday et al., 2002), may function as a "relay team" to control membrane trafficking and ECM remodeling during cytokinesis. To test this hypothesis, we attempted to selectively eliminate actin ring assembly while leaving actin cables intact. This was achieved by deleting the calponin-homology domain (CHD) in Iqg1. As shown previously (Shannon and Li, 1999), the CHD is required for actin ring assembly (Fig. 6 A). 73% of the *IQG1* cells ($n = 60$) with segregated nuclei formed an actin ring, in contrast to only 9% of the *iqg1-CHD*Δ cells ($n = 43$). In addition, Myo1-GFP ring showed no or little constriction before disassembling several minutes after mitotic exit in *iqg1-CHD*Δ cells ($n = 12$), in contrast to the normal constriction and disassembly in *IQG1* cells ($n = 15$; Fig. 6 B; Video 10, compare right to left). 100% of the *IQG1* and *iqg1-CHD*Δ cells with any septal materials at

coupled with membrane trafficking (marked by Myo2-GFP) and PS formation (marked by Chs2-GFP). Cells of strains YKT662 (*MYO2-GFP*) and YEF5762 (*CHS2-GFP*) carrying pRS316-MYO1-mCherry were grown in YPD at 23°C and then imaged by time-lapse microscopy at 23°C with a 1-min interval. Representative montage images of the time-lapse data are shown here. Arrowheads indicate the start of Myo1 ring constriction. (D) Septum morphology in wild-type and different *myo1* mutants. The indicated strains listed in A were processed to visualize septum formation by transmission EM (left) and the orientation of the PS in different strains was measured (diagram; see footnote of Table I for details) and plotted. CW, cell wall; PM, plasma membrane; SS, secondary septum.

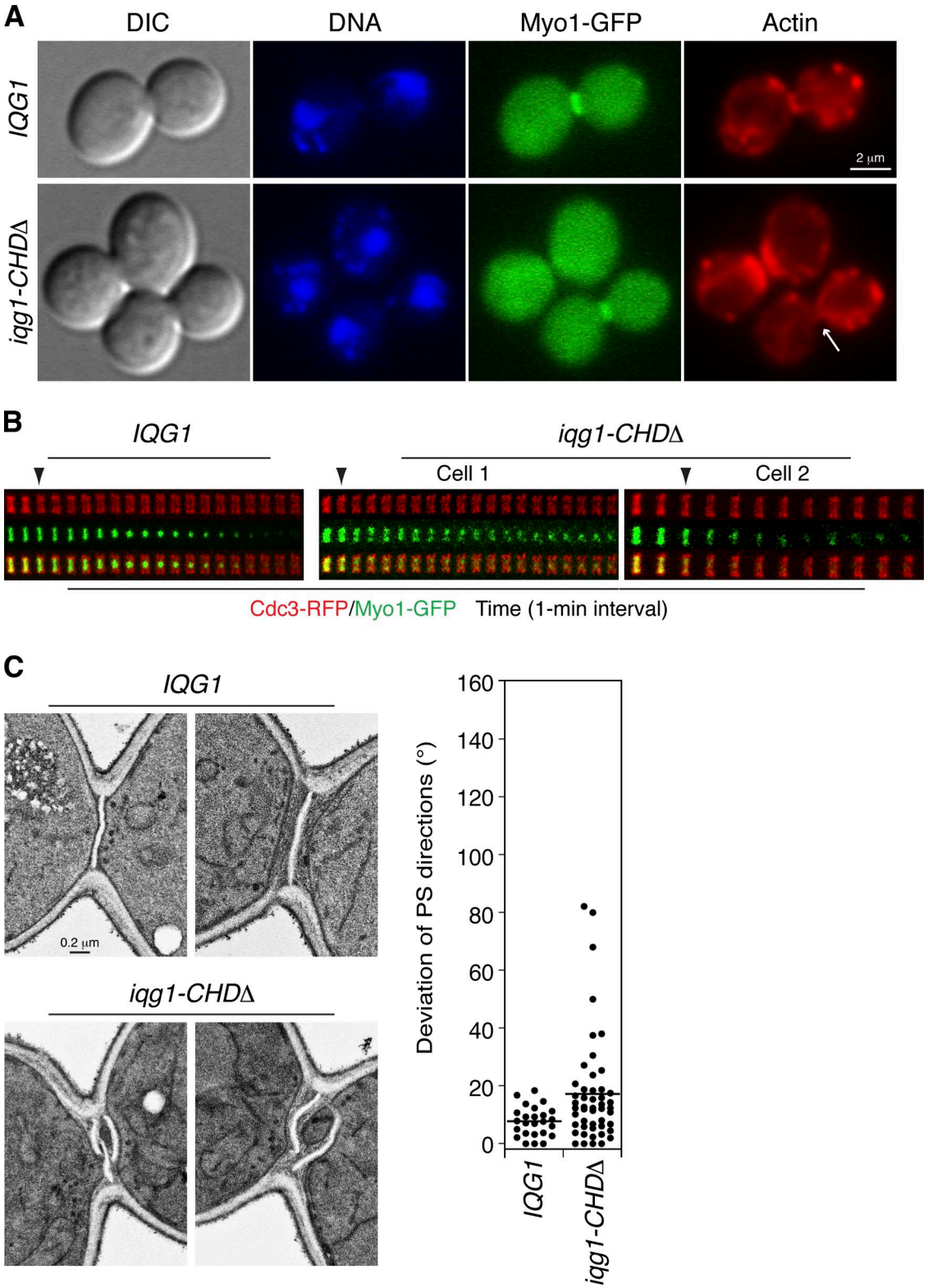

Figure 6. **Actin ring plays a role in guiding PS formation.** (A) Actin ring assembly in *iqg1-CHDΔ* mutant. Cells of strains RNY2594 (*iqg1Δ MYO1-GFP*, pRS315-IQG1-GST) and RNY2595 (*iqg1Δ MYO1-GFP*, pRS315-IQG1[Δ2-411]-GST) were grown in SC-Leu media at 23°C and then fixed and stained for actin and DNA. (B) Abnormal constriction of the Myo1-GFP ring in *iqg1-CHDΔ* mutant. Cells of the strains RNY2596 (*iqg1Δ MYO1-GFP CDC3-mCherry*, pRS315-IQG1-GST) and RNY2597 (*iqg1Δ MYO1-GFP CDC3-mCherry*, pRS315-IQG1[Δ2-411]-GST) were grown in SC-Leu media at 23°C and then imaged by time-lapse microscopy at 23°C with a 1-min interval. Arrowheads indicate septin-hourglass splitting. (C) PS formation in *iqg1-CHDΔ* mutant. PS of the strains listed in A were visualized by transmission EM and the orientation of the PS was quantified as in Fig. 5 D.

the division site formed one or more PS, but the mutant cells were defective in the orientation of the PS (Fig. 6 C). These data suggest that the absence of actin filaments in the AMR causes a slight delay in the initiation of PS formation (as manifested by the lack of Myo1 ring constriction) and a defect in PS guidance. However, the *iqg1-CHD*Δ cells showed much a milder defect in PS orientation than the *myo1*Δ cells did (compare to Fig. 5 D), suggesting that Myo1 plays a major role in PS guidance independently of the actin ring. Together, these results indicate that both Myo1 and actin filaments in the AMR are involved in guiding PS formation during cytokinesis.

Discussion

The kink region of Myo1 tail is required for its targeting to the division site during cytokinesis

In this study, we have shown that full-length Myo1 purified from yeast cells forms a two-headed structure, resembling "conventional" myosins from animal cells. This finding is consistent with the conserved nature of this family of motor proteins, and refutes the speculation that Myo1 might be a single-headed myosin (Bezanilla and Pollard, 2000). It also differs from a previous observation showing that a Myo1 fragment (residues 1044–1569) forms trimers and oligomers but not dimers (Lister et al., 2006). This discrepancy could simply reflect different in vitro biochemical behaviors exhibited by a full-length protein versus its fragments. Whether and how Myo1 is assembled into higher-order structures such as mini- and/or thick filaments and whether this assembly is required for cytokinesis will be investigated in the future.

Myosin IIs from *Dictyostelium*, *Acanthamoeba*, smooth muscle, and nonmuscle cells all display a "kink" or "hinge" in their tails (Trybus, 1991), which may correspond to a region that is predicted to break the helical structure (Fig. S1). The kink is thought to mediate the formation of an auto-inhibitory loop by individual myosin molecules, which can be opened by regulatory light-chain or heavy-chain phosphorylation for myosin activation and higher-order assembly (Trybus, 1991). Myo1 clearly forms a kink in its tail that corresponds to the predicted helix-breaking region, including the TD2 (Fig. S1). The TD2, which was called the putative hinge in a previous study, was reported to be essential for Myo1 contraction (Lister et al., 2006). The underlying assumption was that Myo1 lacking the TD2 could still localize to the division site but fail to contract during cytokinesis. However, here we showed that the TD2 is actually required for Myo1 localization during cytokinesis, as opposed to being required for Myo1 contraction, per se. The difference is that no cell cycle marker for cytokinesis was used in the previous study. These results suggest that the kink region of a myosin II may play important roles in its localization.

Biphasic targeting of Myo1 during the cell cycle: a general feature of myosin II targeting mechanisms?

The tail of a myosin II is responsible for its targeting to the division site (Sabry et al., 1997; Motegi et al., 2004; Lord et al., 2005; Lister et al., 2006; Beach and Egelhoff, 2009). However, it has not been clear what interactions recruit and/or maintain myosins at the division site. We demonstrate here that Myo1 undergoes biphasic targeting through distinct molecular pathways during the cell cycle. Such a mechanism may be generally applicable to the targeting of myosin II to the cleavage furrow in other organisms.

The first-phase targeting accounts for Myo1 localization at the bud neck before cytokinesis. At this stage of the cell cycle, Myo1 may facilitate the retrograde flow of actin cables nucleated at the bud cortex in a motor-dependent manner as described previously (Huckaba et al., 2006; Fig. 7 A). Targeting at this stage requires the function of a molecular pathway (septins → Bni5 → Myo1). Basically, Bni5 interacts directly with the septin Cdc11 (Lee et al., 2002) and with the mTD1 of Myo1, thereby targeting Myo1 to the bud neck before cytokinesis. This may be conceptually similar to the initial targeting of the myosin II Myo2 in fission yeast, which requires Mid1, an anillin-related protein that is important for the selection of division plane as well as for efficient AMR assembly (Motegi et al., 2004; Wu et al., 2006; Huang et al., 2008). In both cases, the initial targeting mechanism acts before cytokinesis and requires some proteins that are not well conserved throughout evolution, such as Bni5 and Mid1. Thus, the initial targeting mechanism may have evolved to accommodate the unique life style of a particular organism.

The second-phase targeting accounts for Myo1 localization at the bud neck during cytokinesis. This targeting requires the function of a distinct molecular pathway (Mlc1 → Iqg1 → Myo1). Mlc1 and Iqg1 are the sole ELC and IQGAP in budding yeast. Mlc1 interacts with Iqg1 and is required for Iqg1 localization to the bud neck (Boyne et al., 2000; Shannon and Li, 2000). We show here that Myo1 targeting during cytokinesis depends on Mlc1 and Iqg1 and this targeting is mediated through the TD2 of Myo1. Importantly, this targeting pathway is coupled with AMR assembly during cytokinesis, as all three components of the pathway are required for actin ring assembly (Epp and Chant, 1997; Bi et al., 1998; Shannon and Li, 2000). One possibility is that the rod-shaped Myo1 tail, after being recruited to the division site by Iqg1, serves as a "template" for actin ring assembly. For example, Myo1 tail could assemble into a higher-order structure that enables Iqg1 and other ring components to distribute more evenly along the circumference of the division site. Alternatively, Myo1 tail may activate Iqg1 to bind to actin filaments via its CHD (Shannon and Li, 1999), thereby promoting actin ring assembly.

In fission yeast, Myo2 can still localize to the cell cortex and promote AMR assembly in *mid1*Δ cells in which the early targeting mechanism is inactivated (Motegi et al., 2004; Wu et al., 2006; Huang et al., 2008), suggesting the existence of a Mid1-independent Myo2 targeting mechanism. This second mechanism likely involves Cdc4, the ELC in fission yeast, as Cdc4 is required for Myo2 localization at the division site whereas Myo2 is not required for Cdc4 localization (Naqvi et al., 1999). Currently, it is not known whether Rng2, the IQGAP in fission yeast, is required for the second-phase targeting by acting in a linear pathway between Cdc4 and Myo2, as Iqg1 does in budding yeast. Importantly, Rng2 is also required for actin ring

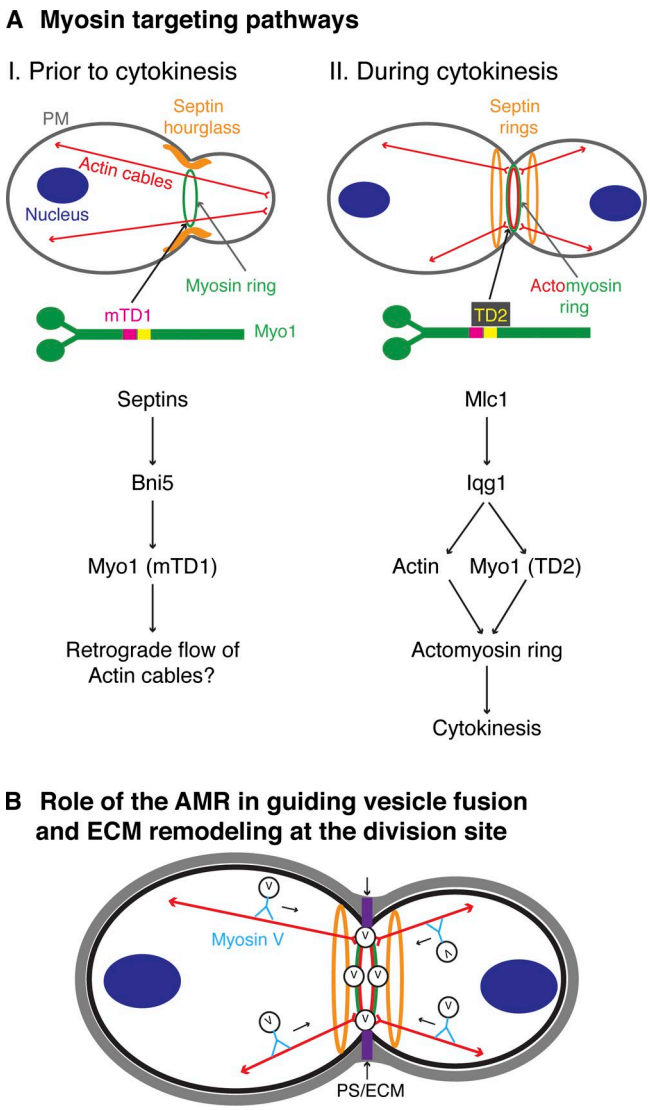

Figure 7. **Biphasic targeting of Myo1 and the guiding role of the actomyosin ring in membrane deposition and ECM remodeling during cytokinesis.** (A) A model for the biphasic targeting of Myo1 during the cell cycle. Myo1 targeting before cytokinesis is mediated solely by the septin-binding protein Bni5. Myo1 targeting during cytokinesis depends on Mlc1 and Iqg1. Iqg1, Myo1, and actin filaments at the bud neck likely define the minimal components of the AMR. (B) A model for the guiding role of the AMR in PS formation. In addition to force generation, the AMR may function as a "compass" to guide membrane deposition and ECM remodeling (PS formation in yeast) during cytokinesis by capturing and distributing vesicles and their cargoes along the division site. This motor-independent guidance role of the AMR is sufficient to ensure membrane closure during cytokinesis for small cells such as budding yeast, but not for the larger ones such as fission yeast and animal cells.

assembly (Eng et al., 1998; Takaine et al., 2009). Thus, the second-phase targeting mechanism in both organisms acts during cytokinesis and appears to involve the conserved proteins ELC and IQGAP. In *Dictyostelium*, the tail-mediated myosin II targeting to the division site depends on its higher-order assembly (Zang and Spudich, 1998; Shu et al., 2003). However, how the assembled myosin II filaments find the cell middle remains unknown. In mammalian cells (Beach and Egelhoff, 2009), the tail of a nonmuscle myosin II localizes to the cleavage furrow independently of its assembly domain presumably by interacting with an unknown protein. It would be intriguing to determine whether ELC and IQGAP are involved in myosin II targeting during cytokinesis in *Dictyostelium* as well as in mammalian cells. Interestingly, the tail of the nonmuscle myosin II in mammalian cells is also able to enrich actin filaments at the division site (Beach and Egelhoff, 2009), suggesting that myosin tail–mediated actin assembly at the division site is not restricted to budding yeast. Taken together, our study and the existing literature suggest that the second-phase targeting mechanism may function to couple myosin localization with AMR assembly during cytokinesis in yeast and beyond.

Actomyosin ring guides membrane deposition and ECM remodeling during cytokinesis

How can a headless AMR assembled by Myo1 tail achieve cytokinesis with reasonable efficiency? To answer this question, we must consider the forces acting at the division site during cytokinesis.

There are two main forces acting at the division site to power plasma membrane ingression during cytokinesis (Fig. 7 B). First, the contractile force generated by the sliding of myosin motor on actin filaments, which depends on the actin-binding and ATPase activities of the myosin head; this force is traditionally thought to be the most important. Second, the force generated by new membrane deposition coupled with centripetal PS formation in yeast and ECM remodeling in animal cells. In budding yeast, PS formation is essential for plasma membrane ingression and thus cytokinesis (Bi, 2001; Schmidt et al., 2002; VerPlank and Li, 2005). In *Caenorhabditis elegans* and mice, the synthesis of the ECM component chondroitin proteoglycan is essential for embryonic cytokinesis (Mizuguchi et al., 2003; Izumikawa et al., 2010).

The two driving forces for membrane closure during cytokinesis must be coordinated in time and space to achieve efficiency and spatial precision. Increasing evidence suggests that AMR assembly and/or contraction and membrane deposition appear to be interdependent in fungal and animal cells (Balasubramanian et al., 2004; Strickland and Burgess, 2004). In budding yeast, the AMR is thought to "guide" membrane deposition and PS formation (Vallen et al., 2000; Bi, 2001), which requires a major contribution from Myo1 and a minor contribution from the actin ring (Figs. 5 and 6). How Myo1 fulfills its guidance role independently of the actin ring remains unknown. The actin ring may fulfill its guidance role as part of a "relay team" with the actin cables (Fig. 7 B). Once post-Golgi vesicles are transported by myosin V along actin cables to the division site (Pruyne et al., 1998), this vesicle–motor system switches to the actin filaments in the AMR, leading to a more even distribution of the vesicles and/or their cargoes such as Chs2 along the division site so that membrane deposition and/or PS formation can occur at a sharply defined position and correct timing, leading to efficient furrowing during cytokinesis. Alternatively, the actin ring may affect PS formation indirectly via its potential role in regulating Myo1 dynamics during cytokinesis. The relay mechanism may also operate during animal cytokinesis, except in this case it involves the switching of vesicle/cargo from a microtubule-based long-range transport system to an actin-based

short-range transport system. A similar mechanism has been hypothesized for cargo transport in nondividing mammalian cells (Ross et al., 2008). Myo1 is also capable of guiding PS formation independently of the actin ring (Fig. 6), suggesting that Myo1 may interact directly with some of the components involved in PS formation (Nishihama et al., 2009). Together, our data indicate that the AMR functions as a structural unit to guide membrane deposition and PS formation during cytokinesis.

In cells carrying Myo1 tail only, the motor domain–dependent force is eliminated while the force generated by membrane deposition and ECM remodeling remains effective, as Myo1 tail is still capable of directing the assembly of a headless AMR that can largely guide PS formation (Fig. 5), which explains, at least in part, why cytokinesis can still occur without the motor domain.

Why is the motor activity of myosin II differentially required for cytokinesis in different organisms?

Why is the motor activity of myosin II not required for cytokinesis in budding yeast but required in fission yeast (Lord et al., 2005) and animal cells (Straight et al., 2003)? The answer may lie in the cell dimension at the division site. The diameter of the division site varies tremendously depending on organisms and cell types, from ∼1 µm in budding yeast (Bi et al., 1998; Lippincott and Li, 1998) to 3.5 µm in fission yeast (Mitchison, 1957), to more than 15–20 µm in animal cells (Carvalho et al., 2009). However, all these organisms or cell types must complete cytokinesis within a similar period of time. Assuming that there is no AMR contraction, for budding yeast, it requires only ∼50 post-Golgi vesicles (the average diameter is 100 nm) for membrane closure during cytokinesis, but would require ∼613 vesicles for fission yeast and ∼20,000 vesicles for an animal cell of 20 µm diameter to achieve the same feat during the same period of time. Thus, even in the complete absence of the AMR such as in *myo1*Δ cells, cytokinesis can still occur in budding yeast (Bi et al., 1998; Schmidt et al., 2002), presumably due to inefficient and AMR-independent vesicle fusion (and septum formation) at the division site. However, for cells with a large division diameter, the motor activity of the myosin II is presumably required to power the invagination of the plasma membrane in order to reduce membrane requirement and achieve efficient cytokinesis within a given period of time. Thus, the basic forces and mechanisms governing cytokinesis are likely the same in yeast and animal cells, but the proportionality of each force in driving cytokinesis to completion may vary depending on the dimension of the division site for each organism or cell type.

Materials and methods

Yeast strains, growth media, and genetic methods

Yeast strains used in this study are listed in Table II. Standard culture media and genetic methods were used throughout this study (Guthrie and Fink, 1991). Where noted, 1 mg/ml 5-fluoroorotic acid (5-FOA; Research Products International) was added to medium to select for the loss of *URA3*-containing plasmids.

Plasmids

Plasmids used in this study are listed in Table III. All primers were purchased from Integrated DNA Technologies through the Cell Center at the University of Pennsylvania (Philadelphia, PA). Sequencing of constructs was performed at the DNA Sequencing Facility, University of Pennsylvania.

Similar to the construction of plasmid pRS316-N-MYO1-GFP, which contains *MYO1* under its own promoter control and carries a NotI $GFP^{F64L/S65T/V163A}$ cassette inserted immediately after the start codon of *MYO1* (Caviston et al., 2003), plasmid pRS316-MYO1-C-GFP was constructed by inserting the same NotI-GFP cassette right before the stop codon of *MYO1*. Both plasmids were used as templates in PCR-mediated mutagenesis to generate plasmids containing different *myo1* deletion alleles presented in Fig. 1 C.

Plasmid pRS316-MYO1-mCherry and YIp211-CDC3-mCherry were constructed by replacing the NotI-GFP cassette in pRS316-MYO1-C-GFP and YIp211-CDC3-GFP (Caviston et al., 2003), respectively, with the NotI-mCherry cassette in the plasmid YIp128-CDC3-mCherry (Gao et al., 2007).

Plasmid pUG23-MYO1 was constructed by PCR-amplifying the *MYO1* ORF from YCp50-MYO1 (Vallen et al., 2000) and gap-repairing into EcoRI-digested pUG23 (provided by J. Hedgemann, Heinrich-Heine-Universität, Düsseldorf, Germany), generating N-terminally tagged *GFP-MYO1* that is under *MET25* promoter control. GFP-Myo1 expressed from this plasmid was able to fully complement the cytokinesis defects of the *myo1*Δ cells even when the cells were grown in standard synthetic media, which contains some methionine that normally represses the *MET25* promoter.

Plasmid pFA6a-mCherry-KanMX6 was constructed by replacing the PacI–AscI fragment carrying *GFP* in plasmid pFA6a-GFP-KanMX6 (Longtine et al., 1998) with the PacI–AscI fragment carrying *mCherry* from pKT355 (or pFA6a-link-mCherry-His3MX6), provided by K. Thorn (University of California, San Francisco, San Francisco, CA).

Plasmids carrying C-terminally TAP-tagged *myo1* alleles were made in several steps. First, a C-terminal TAP tag (CBP-TEV-ProtA) was PCR-amplified from plasmid pBS1479 (Puig et al., 2001), generating a 588-bp *TAP* fragment flanked by symmetrical restriction sites that were introduced in the PCR primers, HindIII–NotI–TAP–NotI–HindIII. This fragment was then digested by HindIII and subscloned into pUC18 (Life Technologies Co.) at the HindIII site, yielding the plasmid pUC18-C-TAP. The correctness of the plasmid was confirmed by restriction-enzyme digestion and sequencing. Plasmids pRS316-MYO1-C-TAP and pRS316-MYO1-TD2Δ-C-TAP were constructed by replacing the NotI-GFP cassette in plasmids pRS316-MYO1-C-GFP and pRS316-MYO1-TD2Δ-C-GFP (see above) with the NotI-TAP cassette isolated from plasmid pUC18-C-TAP.

Plasmids pMAL-MYO1-TD1, pMAL-MYO1-mTD1, and pMAL-MYO1-TD2, which express MBP-tagged Myo1 fragments, were constructed by PCR amplifying *myo1* fragments (*myo1-TD1*, *myo1-mTD1*, and *myo1-TD2*) from the derivatives of pRS316-MYO1-C-GFP described above and subcloning as SalI–PstI fragments (SalI and PstI sites were introduced in the forward and reverse primers, respectively) into SalI- and PstI-digested pMAL-c2 (New England Biolabs, Inc.). Plasmid pGEX-5X-BNI5, which expresses GST-tagged Bni5, was constructed by first PCR amplifying and gap repairing *BNI5 ORF* into the EcoRI site of plasmid pJG-4-5 (Gyuris et al., 1993), and then subcloning a BamHI–XhoI fragment carrying *BNI5 ORF* from pJG4-5-BNI5 into the corresponding sites of pGEX-5X-1 (GE Healthcare).

Plasmid pRS315-IQG1 was constructed by cloning a 7-kb SacI–SalI *IQG1* fragment from p1868 into SacI–SalI-digested pRS315 (Korinek et al., 2000). Plasmid pRS315-IQG1-GST, which expresses C-terminally GST-tagged Iqg1, was constructed by PCR amplifying *GST-His3MX6* from pFA6a-GST-His3MX6 (Longtine et al., 1998) and transforming the PCR product into yeast cells carrying pRS315-IQG1. Candidate plasmids were rescued from yeast cells and transformed into *Escherichia coli* for confirmation by colony PCR and then further confirmed by sequencing. Plasmid pRS315-IQG1(1–697)-GST was constructed in a similar way except that the PCR-amplified *GST-His3MX6* was inserted in-frame after amino acid 697 of Iqg1, resulting in the deletion of residues 698–1495 from Iqg1. Plasmid pRS315-IQG1(Δ2-411)-GST was constructed by a PCR-based method using appropriate mutagenic primers that resulted in the removal of residues 2–411 from Iqg1.

Precise replacement of the endogenous *MYO1* with different *myo1* alleles

We developed a genetic system in which the endogenous *MYO1* can be precisely replaced by any *myo1* allele containing truncation(s) or point mutation(s) without leaving any undesired nucleotides at the *MYO1* locus. Recipient strain Masa1243 [**a** *myo1*Δ*::URA3-KanMX6* (pUG23-MYO1)] was constructed by first using a *URA3* PCR fragment containing 300-bp upstream sequences and 150-bp downstream sequences of *URA3* to replace *MYO1 ORF* in the wild-type strain YEF473A carrying plasmid pUG23-MYO1, and then inserting *KanMX6*, which was PCR

Table II. ***S. cerevisiae*** **strains used in this study**

Strain	Genotype	Reference or source
YEF473A	**a** *his3 leu2 lys2 trp1 ura3*	(Bi and Pringle, 1996)
YEF1820	**a/α** *his3/his3 leu2/leu2 lys2/lys2 trp1/trp1 ura3/ura3 myo1Δ::KanMX6/myo1Δ::HIS3*	(Bi et al., 1998)
YEF1804	As YEF473A except *myo1Δ::KanMX6*	(Bi et al., 1998)
YEF5762	As YEF473A except *CHS2-GFP:His3MX6*	This study[a]
YEF5804	As YEF473A except *CDC3-mCherry:LEU2*	This study[b]
YEF5874	As YEF473A except *CHS2-GFP:His3MX6 CDC3-mCherry:LEU2*	This study[c]
YEF5986	As YEF473A except *MYO2-GFP:His3 CDC3-mCherry:LEU2*	This study[c]
YEF6179	**a** *mlc1-11 MYO1-GFP:KanMX6 CDC3-mCherry:LEU2*	This study[d]
YEF6113	**a** *MYO1-GFP:His3MX6 NUP57-GFP:URA3 his3 leu2 lys2 ura3*	This study[e]
YEF6307	**a** *MYO1-GFP NUP57-GFP:URA3*	This study[f]
YEF6308	**a** *myo1-TD2Δ-GFP NUP57-GFP:URA3*	This study[f]
YEF6309	**a** *myo1-Tail-GFP NUP57-GFP:URA3*	This study[f]
YEF6310	**a** *myo1-TD2-GFP NUP57-GFP:URA3*	This study[f]
YEF6316	**a** *bni5Δ::His3MX6 MYO1-GFP NUP57-GFP:URA3*	This study[f]
YEF6321	**a** *MYO1-GFP BNI5-mCherry:KanMX6*	This study[g]
YEF6322	**a** *bni5Δ::His3MX6 myo1-TD2Δ-GFP*	This study[h]
YEF6323	**a** *bni5Δ::His3MX6 myo1-TD2Δ-GFP CDC3-mCherry:LEU2*	This study[h]
YEF6325	**a** *iqg1Δ::His3MX6 CDC3-mCherry:LEU2* [pRS316-MYO1-C-GFP]	This study[i]
YEF6326	**a** *myo1-mTD1-GFP BNI5-mCherry:KanMX6*	This study[i]
Y5005-8D	As YEF473A except *mlc1-11*	(Luo et al., 2004)
YKT520	As YEF473A except *MYO2-GFP:HIS3*	K. Tanaka
YKT662	As YEF473A except *MYO2-GFP:TRP1*	K. Tanaka
RNY970	As YEF473A except *iqg1Δ::His3MX6* [YCp50-IQG1]	J.R. Pringle
RNY2594	As YEF473A except *iqg1Δ::His3MX6 MYO1-GFP:KanMX6* [pRS315-IQG1-GST]	This study[k]
RNY2595	As YEF473A except *iqg1Δ::His3MX6 MYO1-GFP:KanMX6* [pRS315-IQG1(Δ2-411)-GST]	This study[k]
RNY2596	As YEF473A except *iqg1Δ::His3MX6 MYO1-GFP:KanMX6 CDC3-mCherry:URA3* [pRS315-IQG1-GST]	This study[l]
RNY2597	As YEF473A except *iqg1Δ::His3MX6 MYO1-GFP:KanMX6 CDC3-mCherry:URA3* [pRS315-IQG1(Δ2-411)-GST]	This study[l]
Masa1243	As YEF473A except *myo1Δ::URA3-KanMX6* [pUG23-MYO1]	See text
YJL221A	As YEF473A except *myo1-TD1-GFP*	See text
YJL222A	As YEF473A except *myo1-TD2-GFP*	See text
YJL335A	As YEF473A except *myo1-Tail-GFP*	See text
YJL376A	As YEF473A except *myo1-AD-GFP*	See text
YJL488A	As YEF473A except *myo1-TD2Δ-GFP*	See text
YJL489A	As YEF473A except *myo1-mTD1-GFP*	See text
XDY7	YEF1820 [pRS316-MYO1-C-TAP]	This study
XDY41	As YEF473A except *MYO1-GFP*	See text
XDY99	YEF1820 [pRS316-MYO1-TD2Δ-C-TAP]	This study
XDY154	YEF473A [pRS316-MYO1-TD2-GFP]	This study[m]
XDY173	**a** *mlc1-11* [pRS316-MYO1-TD2-GFP]	This study[m]
XDY189	**a** *myo1-mTD1-GFP BNI5-3HA:His3MX6*	This study[n]
XDY190	**a** *myo1-Tail-GFP BNI5-3HA:His3MX6*	This study[n]
XDY191	**a** *myo1-TD1-GFP BNI5-3HA:His3MX6*	This study[n]
XDY192	**a** *myo1-TD2-GFP BNI5-3HA:His3MX6*	This study[n]
XDY194	**a** *myo1-AD-GFP BNI5-3HA:His3MX6*	This study[n]
XDY211	**a** *myo1-mTD1-GFP BNI5-mCherry:KanMX6* [pRS316-N-*Not*I-MYO1]	This study[o]

Table II. ***S. cerevisiae*** **strains used in this study** *(Continued)*

Strain	Genotype	Reference or source
XDY218	**a** *iqg1Δ::His3MX6* [pRS316-MYO1-TD2-GFP]	This study[p]
XDY254	**a** *MYO1-GFP bni5Δ::His3MX6*	This study[n]
XDY257	**a** *myo1-TD2-GFP bni5Δ::His3MX6*	This study[n]
XDY258	**a** *myo1-mTD1-GFP bni5Δ::His3MX6*	This study[n]
XDY286	**a** *MYO1-GFP CDC3-mCherry:LEU2*	This study[q]
XDY287	**a** *bni5Δ::His3MX6 MYO1-GFP CDC3-mCherry:LEU2*	This study[q]
XDY288	**a** *myo1-Tail-GFP CDC3-mCherry:LEU2*	This study[q]
XDY289	**a** *myo1-TD2Δ-GFP CDC3-mCherry:LEU2*	This study[q]
XDY290	**a** *myo1-TD2-GFP CDC3-mCherry:LEU2*	This study[q]
XDY295	**a** *iqg1Δ::His3MX6* [pRS316-MYO1-TD2-GFP] [pRS315-IQG1-GST]	This study[p]
XDY296	**a** *iqg1Δ::His3MX6* [pRS316-MYO1-TD2-GFP] [pRS315-IQG1(1-697)-GST]	This study[p]
XDY300	**a** *iqg1Δ::His3MX6* [pRS316-MYO1-TD2-GFP] [pRS315-IQG1(Δ2-411)-GST]	This study[p]

[a]Constructed by a PCR-based method (Longtine et al., 1998).

[b]Constructed by transforming BglII-digested YIp128-CDC3-mCherry (Gao et al., 2007) into YEF473A and integrating at the *CDC3* locus.

[c]Constructed by PCR-amplifying *CHS2-GFP:HIS3MX6* and *MYO2-GFP:HIS3* fragments from YEF5762 and YKT520, respectively, and transforming into YEF5804.

[d]Constructed by transforming Y5005-8D with a *MYO1-GFP:KanMX6* fragment that was PCR-amplified from YEF2293 (Luo et al., 2004), followed by integration of BglII-digested YIp128-CDC3-mCherry at the *CDC3* locus.

[e]Constructed by a PCR-based method(Longtine et al., 1998) using plasmids pFA6a-GFP-His3MX6 (Longtine et al., 1998) and pFA6a-GFP-URA3 (provided by C. Burd, University of Pennsylvania, Philadelphia, PA) as templates for tagging *MYO1* and *NUP57*, respectively. The PCR fragments containing *MYO1-GFP:His3MX6* and *NUP57-GFP:URA3* were transformed sequentially into strain RLY1 (Winter et al., 1999).

[f]Constructed by transforming PCR-amplified *NUP57-GFP:URA3* from YEF6113 into strains XDY41, YJL488A, YJL335A, YJL222A, and XDY254, respectively.

[g]Constructed by transforming PCR-amplified *BNI5-mCherry:KanMX6* from XDY211 into XDY41.

[h]Constructed by transforming PCR-amplified *bni5Δ::His3MX6* from XDY254 into YJL448A and XDY289, respectively.

[i]Strain XDY218 was first transformed by BglII-digested YIp128-CDC3-mCherry and then streaked on a SC-Leu + 5-FOA plate to select for the loss of plasmid pRS316-MYO1-TD2-GFP. The resulting strain was then transformed with plasmid pRS316-MYO1-C-GFP.

[j]Constructed by streaking XDY211 on a SC + 5-FOA plate to select for the loss of plasmid pRS316-N-NotI-MYO1.

[k]Strain RNY1264 (*iqg1Δ::His3MX6 MYO1-GFP:KanMX6* [YCp50-IQG1]) was transformed with pRS315-IQG1-GST or pRS315-IQG1(Δ2-411)-GST, and the resulting strains were streaked on a SC-Leu + 5-FOA plate to eliminate YCp50-IQG1.

[l]Constructed by transforming BglII-digested YIp211-CDC3-mCherry into strains RNY2594 and RNY2595 and integrating at the *CDC3* locus.

[m]Constructed by transforming the plasmid into YEF473A and Y5005-8D, respectively.

[n]Strains carrying different *myo1* alleles were transformed with plasmid pRS316-MYO1. The resulting strains were either *3HA*-tagged or deleted for *BNI5* using a PCR-based method (Longtine et al., 1998), and then selected for the loss of the *MYO1* plasmid by growing cells in non-selective YPD medium.

[o]Constructed by transforming a *BNI5-mCherry:KanMX6* fragment that was PCR-amplified from plasmid pFA6a-mCherry-KanMX6 into YJL489A carrying plasmid pRS316-N-*Not*I-MYO1 (Caviston et al., 2003).

[p]Strain RNY970 (shown in the table) was streaked from a SC-His plate onto a SC-His + 5-FOA plate; the resulting single colonies were checked by PCR to confirm the loss of the *IQG1* plasmid. The resulting *iqg1Δ::His3MX6* strain was then transformed with indicated plasmids to generate strains XDY218, XDY295, XDY296, and XDY300.

[q]Strains XDY41, XDY287, YJL335A, YJY222A, and YJY488A were transformed with plasmid pRS316-MYO1. The resulting strains were then transformed with BglII-digested integrative plasmid YIp128-CDC3-mCherry and transformants were selected on SC-Leu plates at 25°C and then grown in non-selective YPD medium to lose the *MYO1* plasmid.

amplified from pFA6a-KanMX6 (Longtine et al., 1998), after the *URA3* at the *myo1Δ* locus.

Plasmids pRS316-N-MYO1-GFP and pRS316-MYO1-C-GFP and their derivatives carrying different *myo1* alleles were digested with SalI and ClaI, and then transformed into Masa1243. The transformation mixtures were plated out on SC-His plates and incubated at 25°C for 2 d. After cells were grown to confluency on SC-His plates, the cells were replicated onto SC-His+ 5-FOA plates to select for Ura^- cells, and then screened for G418 sensitivity on YPD+G418 plates to get Ura^- Kan^s cells in which the *URA3-KanMX6* cassette at the *myo1Δ* locus was replaced by the incoming *myo1* allele. The resulting colonies were then grown in non-selective YPD medium to lose the plasmid pUG23-MYO1.

Purification of TAP-tagged Myo1 from yeast cells

Myo1-C-TAP and Myo1-TD2Δ-C-TAP were purified as described previously (Puig et al., 2001), with some modifications. Eight liters of *myo1Δ* cells carrying pRS316-MYO1-C-TAP or pRS316-MYO1-TD2Δ-C-TAP were grown in SC-Ura medium at 23°C to an OD_{600} = 2.0–3.0, collected by centrifugation, washed twice with water, resuspended into 40.0 ml cell lysis buffer (CLB; 50 mM Hepes-KOH, pH 7.9, 150 mM NaCl, 5 mM $MgCl_2$, 5 mM ATP, 0.1% NP-40, and 2 mM Benzamidine), and added 1.0 ml 100x protease inhibitor cocktail (with stock concentrations of 50 µg/ml leupeptin, 140 µg/ml pepstatin A, 240 µg/ml chymostatin, 1.7 mg/ml aprotinin, 0.25 mg/ml antipain, and 35 µg/ml bestatin) and 0.5 ml 100× phosphatase inhibitor cocktail I (Sigma-Aldrich). The cell suspension was passed

Table III. **Plasmids used in this study**

Plasmid	Description	Reference or source
pUG23-MYO1	*CEN, HIS3, pMET25-yEGFP3, MYO1*	See text
pRS316-N-MYO1-GFP	*CEN, URA3, GFP-MYO1*	(Caviston et al., 2003)
pRS316-MYO1-C-GFP	*CEN, URA3, MYO1-GFP*	See text
pRS316-MYO1-TD2 -GFP	*CEN, URA3, myo1-TD2-GFP*	See text
pRS316-MYO1-TD2Δ-GFP	*CEN, URA3, myo1-TD2Δ-GFP*	See text
pRS316-MYO1-TD1-GFP	*CEN, URA3, myo1-TD1-GFP*	See text
pRS316-MYO1-mTD1-GFP	*CEN, URA3, myo1-mTD1-GFP*	See text
pUC18-C-TAP	*C-TAP*	See text
pRS316-MYO1-C-TAP	*CEN, URA3, MYO1-C-TAP*	See text
pRS316-MYO1-TD2Δ-C-TAP	*CEN, URA3, MYO1-TD2Δ-C-TAP*	See text
pRS316-MYO1-mCherry	*CEN, URA3, MYO1-mCherry*	See text
pMAL-c2	*malE (or N-MBP)*	New England Biolabs
pMAL-MYO1-TD1	*MBP-myo1-TD1*	See text
pMAL-MYO1-mTD1	*MBP-myo1-mTD1*	See text
pMAL-MYO1-TD2	*MBP-myo1-TD2*	See text
pGEX-5X-BNI5	*GST-BNI5*	See text
YIplac128-CDC3-mCherry	*Integrative, LEU2, mCherry (RFP)-CDC3*	(Gao et al., 2007)
YIplac211-CDC3-mCherry	*Integrative, URA3, mCherry (RFP)-CDC3*	See text
pRS315-IQG1	*CEN, LEU2, IQG1*	See text
pRS315-IQG1-GST	*CEN, LEU2, IQG1-GST*	See text
pRS315-IQG1-(1-697)-GST	*CEN, LEU2, iqg1(1-697)-GST*	See text
pRS315-IQG1(Δ2-411)-GST	*CEN, LEU2, iqg1(1, 412-1495)-GST*	See text
YCp50-IQG1	*CEN, URA3, IQG1*	(Korinek et al., 2000)

through a French press three times with a pressure ≤ 1,200 psi to break down the cells, which was followed by centrifugation at 100,000 *g* for 150 min at 4°C to clear the cell lysate. The supernatant was then mixed with 500 µl IgG beads (GE Healthcare), which had been prewashed five times with 5.0 ml CLB. The mixture was incubated with rotation at 4°C overnight. The beads were spun down, washed five times each with 10.0 ml CLB, once with 10.0 ml TEV cleavage buffer (10 mM Hepes-KOH, pH 7.9, 150 mM NaCl, 0.5 mM EDTA, 1 mM DTT, and 0.1% NP-40), resuspended in 1.0 ml TEV cleavage buffer plus 150 U AcTEV Protease (Life Technologies Co.), and then incubated with rotation at 4°C overnight. Approximately 1.0 ml of supernatant containing Myo1 was separated from IgG beads by passing through a column. The column was then washed five times each with 2.0 ml calmodulin binding buffer (CBB; 10 mM Hepes-KOH, pH 7.9, 150 mM NaCl, 1 mM Mg acetate, 1 mM imidazole, 2 mM $CaCl_2$, 10 mM 2-mercaptoethnol, and 0.1% NP-40). The supernatant and the flow-through from the washes were combined, totaling ∼11.0 ml in volume, to which 10 µl 1.0 M $CaCl_2$ was added. This protein solution was mixed with 100 µl Calmodulin Affinity Resin (Agilent Technologies), which had been prewashed three times each with 5.0 ml CBB. The mixture was incubated with rotation at 4°C for 2 h, and then passed through a column, which was followed by three washes each with 10.0 ml CBB. The protein was then eluted 10 times each with 200 µl calmodulin elution buffer (10 mM Hepes-KOH, pH 7.9, 150 mM NaCl, 1 mM imidazole, 20 mM EGTA, 10 mM 2-mercaptoethnol, and 0.1% NP-40).

The combined eluents from the experiments above were passed through Amicon ultra centrifugal filter devices with suitable MWCO (Millipore) to change the buffer into 2x EM buffer (300 mM KCl, 2 mM $MgCl_2$, 2 mM EGTA, 2 mM DTT, 20 mM imidazole-HCl, pH 7.0, and 400 µM ADP), which was then diluted by equal volume of 100% glycerol to make Myo1 preparation in 1x EM buffer for EM observation (see below). The final concentrations of Myo1-C-TAP and myo1-TD2Δ-C-TAP in the EM buffer were ∼10 µg/ml.

Coimmunoprecipitation experiments

100 OD_{600} of yeast cells grown exponentially in SC-His media were disrupted by vortexing with glass beads at 4°C in 500 µl of 1x PBS buffer (137 mM NaCl, 2.7 mM KCl, 10 mM sodium phosphate dibasic, and 2 mM potassium phosphate monobasic, pH 7.4) containing 0.1% NP-40 and a cocktail of protease inhibitors (5x stock) and phosphatase inhibitors (5x cocktail-I stock) for yeast (Sigma-Aldrich). After centrifugation to remove cell debris, the supernatant was used for immunoprecipitation with 1 µl rabbit polyclonal GFP antibody (Abcam) and 30 µl protein A agarose beads (Life Technologies Co.). After incubation at 4°C for 12–16 h, beads were washed five times each with 200 µl lysis buffer without protease and phosphatase inhibitors, and proteins bound to the beads were boiled with 100 µl SDS-sample buffer. The precipitated Myo1-GFP variants, the total Bni5-HA in cell lysates, and the bound fractions of Bni5-HA were analyzed by SDS-PAGE and blotted with anti-GFP, and anti-HA monoclonal antibodies, respectively (Covance).

Production of recombinant proteins and in vitro binding assay

E. coli strain BL21(DE3) containing appropriate constructs for expressing recombinant proteins was grown in 30–600 ml LB plus 100 mg/ml ampicillin at 37°C to OD_{600} ≤ 1.0. Expression of recombinant proteins was induced with 1 mM IPTG at 23°C for 3 h. Cells were then collected by centrifugation, washed twice with water, resuspended into 5–20 ml cell lysis buffer (CLB [the CLB for MBP-tagged proteins: 20 mM Tris-HCl, pH 8.0, 100 mM NaCl, 5 mM EDTA, 5 mM DTT, 0.1% NP-40, and 2× complete protein inhibitor cocktail tablets; Roche Diagnostics Co.; the CLB for GST-tagged protein: 1x PBS, 5 mM EDTA, 5 mM DTT, 0.1% NP-40, and 2× complete protein inhibitor cocktail]). Cells were then broken by sonicating for 7 x 15 s with 15-s interval on ice, centrifuged at 15,000 rpm for 20 min at 4°C. Supernatant was collected and incubated with prewashed amylose beads (New England Biolabs, Inc.) for MBP-tagged proteins or glutathione Sepharose 4B beads (GE Healthcare) for GST-tagged proteins at 4°C for 1 h. Beads were then washed three times each with 5.0 ml corresponding CLB buffer. MBP-tagged proteins were resuspended in 1.0 ml CLB. GST-tagged proteins were eluted five times each with 200 µl elution buffer, which is the CLB for MBP-tagged proteins, except containing 10 mM reduced glutathione and lacking the protease inhibitors.

The concentrations of the purified recombinant proteins were estimated by comparing the sample proteins to bovine serum albumin (BSA) of known concentrations by SDS-PAGE analysis, followed by staining the gel with simple blue (Life Technologies Co.). Approximately 40 µg MBP-tagged proteins that were still bound on beads were added to different 1.5-ml Eppendorf tubes, the amount of beads was normalized by adding more prewashed beads, and then incubated with 500 µl 5% BSA at 4°C for 1 h to block nonspecific binding by the beads. After a brief centrifugation to pellet the beads and remove the supernatant, the beads were mixed with 10 µg GST-tagged protein. The CLB for MBP-tagged proteins without the protease inhibitors was added to the reaction to make the final volume of 500 µl. The binding reaction was incubated with rotation at 4°C for 1 h, and

then spun down to pellet the beads, which were then washed three times each with 500 µl binding buffer at 4°C for 10 min. The final protein complexes were eluted by adding 100 µl 2x SDS sample buffer and boiled for 5 min, resolved by SDS-PAGE and analyzed by Western blotting.

For EM observation, MBP-myo1-Tail-TD2Δ was purified essentially as described above except that 600 ml culture was used and the recombinant protein was eluted from the amylose beads using maltose. The buffer for the protein suspension was changed into 1x EM buffer as described for TAP-tagged Myo1 above. The final concentration of MBP-myo1-Tail-TD2Δ was ~100 mg/ml.

Light and EM

All cells were in exponential phase for imaging experiments. Differential interference contrast (DIC) and fluorescence microscopy were performed using a microscope (model E800; Nikon) equipped with a Plan Apochromat 60x/1.40 NA oil immersion objective (Nikon), a CCD camera (model C4742-95; Hamamatsu Photonics), and Image-Pro Plus software (Media Cybernetics).

For time-lapse microscopy, cells were spotted onto a thin layer of SC medium + 2% agarose on a microscope slide. Individual cells were followed at 1-min interval using IPLab software (BD) and a spinning-disk confocal microscope system comprising a scanner (CSU 10; Yokogawa), a microscope (IX 71; Olympus), a Plan S-Apo 100x/1.4 NA oil immersion objective (Olympus), and an ImagEM back-thinned EM CCD camera (C9100-13; Hamamatsu Photonics); components were integrated by Bio-Vision Technologies. Diode lasers for excitation (488 nm for GFP; 561 nm for RFP) were housed in a launch constructed by Spectral Applied Research. For each time point, 10 z-sections were acquired at 0.2- or 0.3-mm increments at 23°C. Maximum projection of images for each time point was generated using IPLab software. The contrast and the brightness of the images were enhanced using NIH ImageJ, and the finalized time-lapse data were presented as montages using ImageJ or as movies using MetaMorph (MDS Analytical Technologies). The constriction rate of Myo1 ring was determined as the diameter of Myo1 ring before constriction minus the diameter of the first Myo1 dot near the end of constriction divided by the time required to undergo this change. Only cells with symmetric Myo1 constriction were used in the calculation.

For observation of Myo1-C-TAP, Myo1-TD2D-C-TAP, and MBP-myo1-Tail-TD2D structures by rotary-shadowing EM, 5–10.0 µl of each protein suspensions in 1x EM buffer was sprayed on freshly split mica (Tyler and Branton, 1980; Rock et al., 2005). The droplets were dried under vacuum, rotary-shadowed with platinum at an angle of 7°, and replicated with carbon in a freeze-fracture apparatus (model BFA 400; Balzers Spa). The replicas were photographed in an electron microscope (model 410; Philips) operating at 60 kV. The negatives were digitally scanned at 1,000 ppi, and the tail length of Myo1 and its derivatives was determined by measuring individual molecules from the head–tail junction to the C-terminal end using Photoshop software.

For observation of PS in different *myo1* and *iqg1* mutants by transmission EM, cells were fixed and processed as described previously (Nishihama et al., 2009).

Latrunculin A treatment and actin staining

Cells were grown in YPD medium to exponential phase (OD_{600} = 0.5–1.0) and then treated with 1/100 volume of 20 mM latrunculin A (LatA) (Wako Chemicals USA, Inc.) or DMSO (solvent in which LatA was dissolved) for 30 min, then added 1/10 volume of 37% formaldehyde for fixation at 24°C for 30 min. Cells were then washed with PBS, permeabilized with PBS plus 0.2% Triton X-100, and stained for F-actin and DNA as described previously (Bi et al., 1998).

Online supplemental material

Fig. S1 shows coiled-coil profiles of myosin IIs from different organisms or cell types. Fig. S2 shows myo1-TD2-GFP in *bni5*Δ and LatA-treated cells. Fig. S3 shows disassembly defect of Myo1 tail during and after cytokinesis, and quantitative analysis of constriction behaviors of the full-length Myo1 in wild-type and *bni5*Δ cells as well as in cells carrying different *myo1* alleles. Fig. S4 shows actin ring assembly in *bni5*Δ and different *myo1* mutant cells, and the timing of Myo2 and Chs2 localization with respect to septin-hourglass splitting during the cell cycle. Video 1 shows localization of Bni5 versus Myo1 and myo1-mTD1 during the cell cycle. Video 2 shows the disappearance of full-length Myo1 from the bud neck at the onset of cytokinesis in *mlc1-11* and *iqg1*Δ cells. Video 3 shows the constriction patterns of the rings formed by full-length Myo1 versus its tail. Video 4 shows the disappearance of the myo1-TD2Δ-GFP ring from the bud neck before the onset of cytokinesis. Video 5 shows the complete failure of myo1-TD2Δ-GFP localization to the bud neck in *bni5*Δ cells. Video 6 shows the localization of Myo1 in *bni5*Δ cells versus localization of myo1-TD2 during the cell cycle. Video 7 shows three-dimensional construction of the actin ring in a *myo1-Tail* cell. Video 8 shows the localization of Myo1 versus Myo2 and Chs2 during the cell cycle. Video 9 shows the localization of Myo2 and Chs2 versus Cdc3 during the cell cycle. Video 10 shows the constriction patterns of Myo1 ring in the presence of full-length *IQG1* versus *iqg1(Δ2-411)*. Online supplemental material is available at http://www.jcb.org/cgi/content/full/jcb.201005134/DC1.

We would like to thank Drs. J.R. Pringle, J. Hedgemann, J. Chant, J. Thorner, and M. Longtine for plasmids and strains; J.R. Pringle, M. Longtine, L. Thé, and X. Gao for sharing unpublished results; A. Stout and C. Fu for their help with imaging and analysis; J. Hanna for technical assistance; M. Lord, M. Ostap, and P. Tran for critically reading the manuscript; and the members of Bi laboratory for discussions.

This work was supported by the National Institutes of Health grants GM59216 (to E. Bi), GM31006 (to J.R. Pringle), P01-AR051174 (to C. Franzini-Armstrong) and by the American Cancer Society grant RSG-02-039-01-CSM (to E. Bi).

Submitted: 25 May 2010
Accepted: 29 November 2010

References

Ayscough, K.R., J. Stryker, N. Pokala, M. Sanders, P. Crews, and D.G. Drubin. 1997. High rates of actin filament turnover in budding yeast and roles for actin in establishment and maintenance of cell polarity revealed using the actin inhibitor latrunculin-A. *J. Cell Biol.* 137:399–416. doi:10.1083/jcb.137.2.399

Balasubramanian, M.K., E. Bi, and M. Glotzer. 2004. Comparative analysis of cytokinesis in budding yeast, fission yeast and animal cells. *Curr. Biol.* 14:R806–R818. doi:10.1016/j.cub.2004.09.022

Beach, J.R., and T.T. Egelhoff. 2009. Myosin II recruitment during cytokinesis independent of centralspindlin-mediated phosphorylation. *J. Biol. Chem.* 284:27377–27383. doi:10.1074/jbc.M109.028316

Bezanilla, M., and T.D. Pollard. 2000. Myosin-II tails confer unique functions in *Schizosaccharomyces pombe*: characterization of a novel myosin-II tail. *Mol. Biol. Cell.* 11:79–91.

Bi, E. 2001. Cytokinesis in budding yeast: the relationship between actomyosin ring function and septum formation. *Cell Struct. Funct.* 26:529–537. doi:10.1247/csf.26.529

Bi, E., and J.R. Pringle. 1996. *ZDS1* and *ZDS2*, genes whose products may regulate Cdc42p in *Saccharomyces cerevisiae*. *Mol. Cell. Biol.* 16:5264–5275.

Bi, E., P. Maddox, D.J. Lew, E.D. Salmon, J.N. McMillan, E. Yeh, and J.R. Pringle. 1998. Involvement of an actomyosin contractile ring in *Saccharomyces cerevisiae* cytokinesis. *J. Cell Biol.* 142:1301–1312. doi:10.1083/jcb.142.5.1301

Boyne, J.R., H.M. Yosuf, P. Bieganowski, C. Brenner, and C. Price. 2000. Yeast myosin light chain, Mlc1p, interacts with both IQGAP and class II myosin to effect cytokinesis. *J. Cell Sci.* 113:4533–4543.

Carvalho, A., A. Desai, and K. Oegema. 2009. Structural memory in the contractile ring makes the duration of cytokinesis independent of cell size. *Cell.* 137:926–937. doi:10.1016/j.cell.2009.03.021

Caviston, J.P., M. Longtine, J.R. Pringle, and E. Bi. 2003. The role of Cdc42p GTPase-activating proteins in assembly of the septin ring in yeast. *Mol. Biol. Cell.* 14:4051–4066. doi:10.1091/mbc.E03-04-0247

Eng, K., N.I. Naqvi, K.C. Wong, and M.K. Balasubramanian. 1998. Rng2p, a protein required for cytokinesis in fission yeast, is a component of the actomyosin ring and the spindle pole body. *Curr. Biol.* 8:611–621. doi:10.1016/S0960-9822(98)70248-9

Epp, J.A., and J. Chant. 1997. An IQGAP-related protein controls actin-ring formation and cytokinesis in yeast. *Curr. Biol.* 7:921–929. doi:10.1016/S0960-9822(06)00411-8

Evangelista, M., D. Pruyne, D.C. Amberg, C. Boone, and A. Bretscher. 2002. Formins direct Arp2/3-independent actin filament assembly to polarize cell growth in yeast. *Nat. Cell Biol.* 4:32–41. doi:10.1038/ncb718

Gao, X.D., L.M. Sperber, S.A. Kane, Z. Tong, A.H. Tong, C. Boone, and E. Bi. 2007. Sequential and distinct roles of the cadherin domain-containing protein Axl2p in cell polarization in yeast cell cycle. *Mol. Biol. Cell.* 18:2542–2560. doi:10.1091/mbc.E06-09-0822

Guthrie, C., and G.R. Fink. 1991. Guide to Yeast Genetics and Molecular Biology. *Methods Enzymol.* Vol. 194. 933 pp.

Gyuris, J., E. Golemis, H. Chertkov, and R. Brent. 1993. Cdi1, a human G1 and S phase protein phosphatase that associates with Cdk2. *Cell.* 75:791–803. doi:10.1016/0092-8674(93)90498-F

Huang, Y., H. Yan, and M.K. Balasubramanian. 2008. Assembly of normal actomyosin rings in the absence of Mid1p and cortical nodes in fission yeast. *J. Cell Biol.* 183:979–988. doi:10.1083/jcb.200806151

Huckaba, T.M., T. Lipkin, and L.A. Pon. 2006. Roles of type II myosin and a tropomyosin isoform in retrograde actin flow in budding yeast. *J. Cell Biol.* 175:957–969. doi:10.1083/jcb.200609155

Izumikawa, T., N. Kanagawa, Y. Watamoto, M. Okada, M. Saeki, M. Sakano, K. Sugahara, K. Sugihara, M. Asano, and H. Kitagawa. 2010. Impairment of embryonic cell division and glycosaminoglycan biosynthesis in glucuronyltransferase-I-deficient mice. *J. Biol. Chem.* 285:12190–12196. doi:10.1074/jbc.M110.100941

Joo, E., C.W. Tsang, and W.S. Trimble. 2005. Septins: traffic control at the cytokinesis intersection. *Traffic.* 6:626–634. doi:10.1111/j.1600-0854.2005.00305.x

Joo, E., M.C. Surka, and W.S. Trimble. 2007. Mammalian SEPT2 is required for scaffolding nonmuscle myosin II and its kinases. *Dev. Cell.* 13:677–690. doi:10.1016/j.devcel.2007.09.001

Ko, N., R. Nishihama, G.H. Tully, D. Ostapenko, M.J. Solomon, D.O. Morgan, and J.R. Pringle. 2007. Identification of yeast IQGAP (Iqg1p) as an anaphase-promoting-complex substrate and its role in actomyosin-ring-independent cytokinesis. *Mol. Biol. Cell.* 18:5139–5153. doi:10.1091/mbc.E07-05-0509

Korinek, W.S., E. Bi, J.A. Epp, L. Wang, J. Ho, and J. Chant. 2000. Cyk3, a novel SH3-domain protein, affects cytokinesis in yeast. *Curr. Biol.* 10:947–950. doi:10.1016/S0960-9822(00)00626-6

Lee, P.R., S. Song, H.S. Ro, C.J. Park, J. Lippincott, R. Li, J.R. Pringle, C. De Virgilio, M.S. Longtine, and K.S. Lee. 2002. Bni5p, a septin-interacting protein, is required for normal septin function and cytokinesis in *Saccharomyces cerevisiae. Mol. Cell. Biol.* 22:6906–6920. doi:10.1128/MCB.22.19.6906-6920.2002

Lippincott, J., and R. Li. 1998. Sequential assembly of myosin II, an IQGAP-like protein, and filamentous actin to a ring structure involved in budding yeast cytokinesis. *J. Cell Biol.* 140:355–366. doi:10.1083/jcb.140.2.355

Lippincott, J., K.B. Shannon, W. Shou, R.J. Deshaies, and R. Li. 2001. The Tem1 small GTPase controls actomyosin and septin dynamics during cytokinesis. *J. Cell Sci.* 114:1379–1386.

Lister, I.M., N.J. Tolliday, and R. Li. 2006. Characterization of the minimum domain required for targeting budding yeast myosin II to the site of cell division. *BMC Biol.* 4:19. doi:10.1186/1741-7007-4-19

Longtine, M.S., and E. Bi. 2003. Regulation of septin organization and function in yeast. *Trends Cell Biol.* 13:403–409. doi:10.1016/S0962-8924(03)00151-X

Longtine, M.S., A. McKenzie III, D.J. Demarini, N.G. Shah, A. Wach, A. Brachat, P. Philippsen, and J.R. Pringle. 1998. Additional modules for versatile and economical PCR-based gene deletion and modification in *Saccharomyces cerevisiae. Yeast.* 14:953–961. doi:10.1002/(SICI)1097-0061(199807)14:10<953::AID-YEA293>3.0.CO;2-U

Lord, M., E. Laves, and T.D. Pollard. 2005. Cytokinesis depends on the motor domains of myosin-II in fission yeast but not in budding yeast. *Mol. Biol. Cell.* 16:5346–5355. doi:10.1091/mbc.E05-07-0601

Luo, J., E.A. Vallen, C. Dravis, S.E. Tcheperegine, B.L. Drees, and E. Bi. 2004. Identification and functional analysis of the essential and regulatory light chains of the only type II myosin Myo1p in *Saccharomyces cerevisiae. J. Cell Biol.* 165:843–855. doi:10.1083/jcb.200401040

Lupas, A., M. Van Dyke, and J. Stock. 1991. Predicting coiled coils from protein sequences. *Science.* 252:1162–1164. doi:10.1126/science.252.5009.1162

Mitchison, J.M. 1957. The growth of single cells. I. *Schizosaccharomyces pombe. Exp. Cell Res.* 13:244–262. doi:10.1016/0014-4827(57)90005-8

Mizuguchi, S., T. Uyama, H. Kitagawa, K.H. Nomura, K. Dejima, K. Gengyo-Ando, S. Mitani, K. Sugahara, and K. Nomura. 2003. Chondroitin proteoglycans are involved in cell division of *Caenorhabditis elegans. Nature.* 423:443–448. doi:10.1038/nature01635

Moseley, J.B., and B.L. Goode. 2006. The yeast actin cytoskeleton: from cellular function to biochemical mechanism. *Microbiol. Mol. Biol. Rev.* 70:605–645. doi:10.1128/MMBR.00013-06

Motegi, F., M. Mishra, M.K. Balasubramanian, and I. Mabuchi. 2004. Myosin-II reorganization during mitosis is controlled temporally by its dephosphorylation and spatially by Mid1 in fission yeast. *J. Cell Biol.* 165:685–695. doi:10.1083/jcb.200402097

Naqvi, N.I., K. Eng, K.L. Gould, and M.K. Balasubramanian. 1999. Evidence for F-actin-dependent and -independent mechanisms involved in assembly and stability of the medial actomyosin ring in fission yeast. *EMBO J.* 18:854–862. doi:10.1093/emboj/18.4.854

Nishihama, R., J.H. Schreiter, M. Onishi, E.A. Vallen, J. Hanna, K. Moravcevic, M.F. Lippincott, H. Han, M.A. Lemmon, J.R. Pringle, and E. Bi. 2009. Role of Inn1 and its interactions with Hof1 and Cyk3 in promoting cleavage furrow and septum formation in *S. cerevisiae. J. Cell Biol.* 185:995–1012. doi:10.1083/jcb.200903125

Pruyne, D.W., D.H. Schott, and A. Bretscher. 1998. Tropomyosin-containing actin cables direct the Myo2p-dependent polarized delivery of secretory vesicles in budding yeast. *J. Cell Biol.* 143:1931–1945. doi:10.1083/jcb.143.7.1931

Puig, O., F. Caspary, G. Rigaut, B. Rutz, E. Bouveret, E. Bragado-Nilsson, M. Wilm, and B. Séraphin. 2001. The tandem affinity purification (TAP) method: a general procedure of protein complex purification. *Methods.* 24:218–229. doi:10.1006/meth.2001.1183

Rock, R.S., B. Ramamurthy, A.R. Dunn, S. Beccafico, B.R. Rami, C. Morris, B.J. Spink, C. Franzini-Armstrong, J.A. Spudich, and H.L. Sweeney. 2005. A flexible domain is essential for the large step size and processivity of myosin VI. *Mol. Cell.* 17:603–609. doi:10.1016/j.molcel.2005.01.015

Ronen, D., and S. Ravid. 2009. Myosin II tailpiece determines its paracrystal structure, filament assembly properties, and cellular localization. *J. Biol. Chem.* 284:24948–24957. doi:10.1074/jbc.M109.023754

Ross, J.L., M.Y. Ali, and D.M. Warshaw. 2008. Cargo transport: molecular motors navigate a complex cytoskeleton. *Curr. Opin. Cell Biol.* 20:41–47. doi:10.1016/j.ceb.2007.11.006

Sabry, J.H., S.L. Moores, S. Ryan, J.-H. Zang, and J.A. Spudich. 1997. Myosin heavy chain phosphorylation sites regulate myosin localization during cytokinesis in live cells. *Mol. Biol. Cell.* 8:2605–2615.

Sagot, I., S.K. Klee, and D. Pellman. 2002. Yeast formins regulate cell polarity by controlling the assembly of actin cables. *Nat. Cell Biol.* 4:42–50.

Schmidt, M., B. Bowers, A. Varma, D.-H. Roh, and E. Cabib. 2002. In budding yeast, contraction of the actomyosin ring and formation of the primary septum at cytokinesis depend on each other. *J. Cell Sci.* 115:293–302.

Shannon, K.B., and R. Li. 1999. The multiple roles of Cyk1p in the assembly and function of the actomyosin ring in budding yeast. *Mol. Biol. Cell.* 10:283–296.

Shannon, K.B., and R. Li. 2000. A myosin light chain mediates the localization of the budding yeast IQGAP-like protein during contractile ring formation. *Curr. Biol.* 10:727–730. doi:10.1016/S0960-9822(00)00539-X

Shu, S., X. Liu, and E.D. Korn. 2003. Dictyostelium and Acanthamoeba myosin II assembly domains go to the cleavage furrow of Dictyostelium myosin II-null cells. *Proc. Natl. Acad. Sci. USA.* 100:6499–6504. doi:10.1073/pnas.0732155100

Straight, A.F., A. Cheung, J. Limouze, I. Chen, N.J. Westwood, J.R. Sellers, and T.J. Mitchison. 2003. Dissecting temporal and spatial control of cytokinesis with a myosin II Inhibitor. *Science.* 299:1743–1747. doi:10.1126/science.1081412

Strickland, L.I., and D.R. Burgess. 2004. Pathways for membrane trafficking during cytokinesis. *Trends Cell Biol.* 14:115–118. doi:10.1016/j.tcb.2004.01.006

Takaine, M., O. Numata, and K. Nakano. 2009. Fission yeast IQGAP arranges actin filaments into the cytokinetic contractile ring. *EMBO J.* 28:3117–3131. doi:10.1038/emboj.2009.252

Tolliday, N., L. VerPlank, and R. Li. 2002. Rho1 directs formin-mediated actin ring assembly during budding yeast cytokinesis. *Curr. Biol.* 12:1864–1870. doi:10.1016/S0960-9822(02)01238-1

Trybus, K.M. 1991. Assembly of cytoplasmic and smooth muscle myosins. *Curr. Opin. Cell Biol.* 3:105–111. doi:10.1016/0955-0674(91)90172-U

Tully, G.H., R. Nishihama, J.R. Pringle, and D.O. Morgan. 2009. The anaphase-promoting complex promotes actomyosin-ring disassembly during cytokinesis in yeast. *Mol. Biol. Cell.* 20:1201–1212. doi:10.1091/mbc.E08-08-0822

Tyler, J.M., and D. Branton. 1980. Rotary shadowing of extended molecules dried from glycerol. *J. Ultrastruct. Res.* 71:95–102. doi:10.1016/S0022-5320(80)90098-2

Vallen, E.A., J. Caviston, and E. Bi. 2000. Roles of Hof1p, Bni1p, Bnr1p, and myo1p in cytokinesis in *Saccharomyces cerevisiae. Mol. Biol. Cell.* 11:593–611.

VerPlank, L., and R. Li. 2005. Cell cycle-regulated trafficking of Chs2 controls actomyosin ring stability during cytokinesis. *Mol. Biol. Cell.* 16:2529–2543. doi:10.1091/mbc.E04-12-1090

Winter, D.C., E.Y. Choe, and R. Li. 1999. Genetic dissection of the budding yeast Arp2/3 complex: a comparison of the *in vivo* and structural roles of individual subunits. *Proc. Natl. Acad. Sci. USA.* 96:7288–7293. doi:10.1073/pnas.96.13.7288

Wu, J.Q., V. Sirotkin, D.R. Kovar, M. Lord, C.C. Beltzner, J.R. Kuhn, and T.D. Pollard. 2006. Assembly of the cytokinetic contractile ring from a broad band of nodes in fission yeast. *J. Cell Biol.* 174:391–402. doi:10.1083/jcb.200602032

Zang, J.H., and J.A. Spudich. 1998. Myosin II localization during cytokinesis occurs by a mechanism that does not require its motor domain. *Proc. Natl. Acad. Sci. USA.* 95:13652–13657. doi:10.1073/pnas.95.23.13652

Correction: Biphasic targeting and cleavage furrow ingression directed by the tail of a myosin II

Xiaodong Fang, Jianying Luo, Ryuichi Nishihama, Carsten Wloka, Christopher Dravis, Mirko Travaglia, Masayuki Iwase, Elizabeth A. Vallen, and Erfei Bi

Vol. 191 No. 7, December 27, 2010. Pages 1333–1350.

After publication of the paper, the authors discovered an error in figure preparation. In Fig. 3 B of the original manuscript, the authors used the same *mlc-11* GFP channel kymograph in both the *mlc1-11* (left) and *iqg1Δ* (right) panels. The authors have provided the corrected image and the affected legends (Fig. 3 and Video 2). This error in figure preparation does not impact the conclusions of the paper.

The HTML and PDF versions of the article have been corrected. The error remains only in the print version.

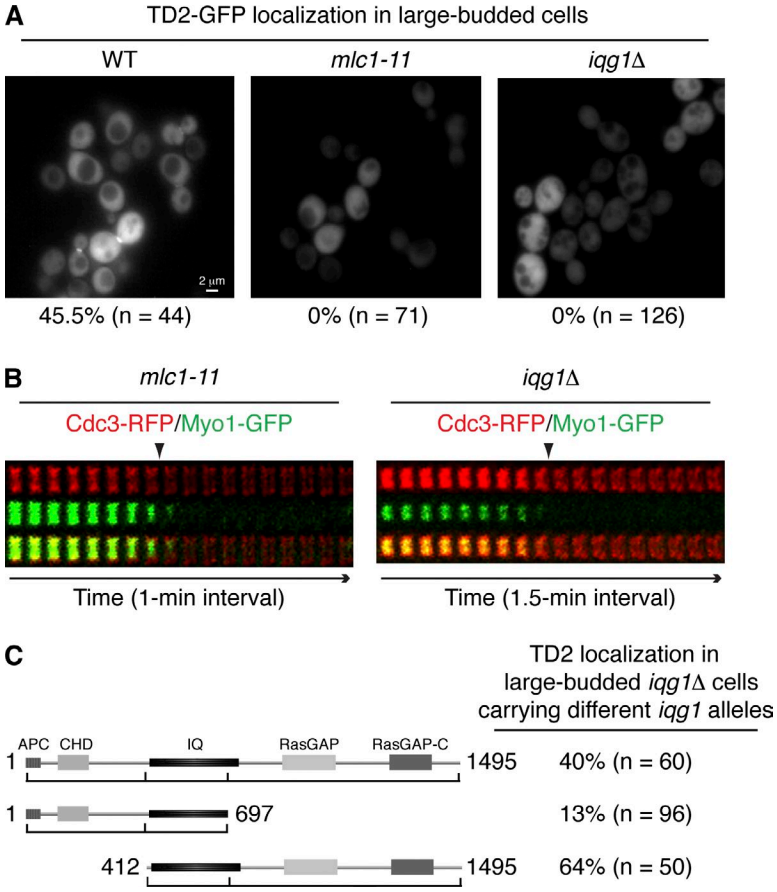

Figure 3. **Myo1 targeting during cytokinesis depends on Mlc1 and Iqg1.** (A) myo1-TD2 localization depends on Mlc1 and Iqg1. Wild-type (WT) (XDY154), *mlc1-11* (XDY173), and *iqg1Δ* (XDY218) cells carrying plasmid pRS316-MYO1-TD2-GFP were grown in SC-Ura medium at 23°C and then examined for myo1-TD2 localization. (B) Full-length Myo1 localization depends on Mlc1 and Iqg1. Strains YEF6179 (*mlc1-11 MYO1-GFP CDC3-RFP*; left) and YEF6325 (*iqg1Δ CDC3-RFP*, pRS316-MYO1-C-GFP; right) were grown in liquid SC-Leu media at 23°C and then imaged by 3D dual-color time-lapse microscopy at 23°C with indicated intervals. Montage images of the GFP, RFP, and merged channels from the representative time-lapse data are shown here. Arrowheads indicate the splitting of septin hourglass into two cortical rings, which coincides with mitotic exit and the onset of cytokinesis. (C) myo1-TD2 localization in cells containing different *iqg1* alleles. Plasmid pRS315 derivatives carrying the indicated *iqg1* alleles (see Table III) were transformed into strain XDY218. Transformants were grown in SC-Ura-Leu medium at 23°C and then quantified for myo1-TD2 localization. APC, APC/C recognition site; CHD, calponin-homology domain; IQ, IQ motifs; Ras-GAP, RasGAP-related domain; RasGAP-C, RasGAP C terminus–related domain.

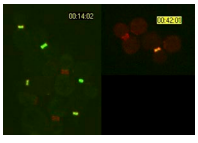

Video 2. **Full-length Myo1 disappears from the bud neck at the onset of cytokinesis in *mlc1-11* and *iqg1Δ* cells.** (Left) Strain: YEF6179 (**a** *mlc1-11 MYO1-GFP CDC3-mCherry:LEU2*). Green, Myo1-GFP; red, Cdc3-RFP. 1-min time-lapse interval is shown. (Right) Strain: YEF6325 (**a** *iqg1Δ CDC3-mCherry:LEU2*, pRS316-MYO1-C-GFP). Green, Myo1-GFP; red, Cdc3-RFP. 1.5-min time-lapse interval is shown.